FACULTY
OF MECHANICAL
ENGINEERING
CTU IN PRAGUE

CFD Modelling of Horizontal Water Film Evaporation

Master's Thesis

Bc. Radomír Kalinay

Prague, 2017

ČESKÉ VYSOKÉ UČENÍ TECHNICKÉ V PRAZE

ZADÁNÍ DIPLOMOVÉ PRÁCE

I. OSOBNÍ A STUDIJNÍ ÚDAJE

Příjmení: **Kalinay** Jméno: **Radomír** Osobní číslo: **408895**

Fakulta/ústav: **Fakulta strojní**

Zadávající katedra/ústav: **Ústav mechaniky tekutin a termodynamiky**

Studijní program: **Strojní inženýrství**

Studijní obor: **Aplikovaná mechanika**

II. ÚDAJE K DIPLOMOVÉ PRÁCI

Název diplomové práce:

CFD modelování vypařování z horizontálního vodního filmu

Název diplomové práce anglicky:

CFD Modelling of Horizontal Water Film Evaporation

Pokyny pro vypracování:

Discuss available models applicable in the field of CFD modelling of horizontal water film evaporation.
Describe validation experiment and formulate the problem for the numerical solution. Describe used mathematical models.
Concentrate on the post-processing like model and the model based on direct application of Fick's law.
Discuss an influence of radiation.
Test an influence of used computational mesh.
Discuss obtained results and make a comparison with experimental data.
Scope of accompanying report: about 60 pages

Seznam doporučené literatury:

as recommended by the supervisor

Jméno a pracoviště vedoucí(ho) diplomové práce:

Ing. Tomáš Hyhlík Ph.D., 12112

Jméno a pracoviště druhé(ho) vedoucí(ho) nebo konzultanta(ky) diplomové práce:

Datum zadání diplomové práce: **27.04.2017** Termín odevzdání diplomové práce: **14.08.2017**

Platnost zadání diplomové práce: **26.10.2018**

Podpis vedoucí(ho) práce	Podpis vedoucí(ho) ústavu/katedry	Podpis děkana(ky)

III. PŘEVZETÍ ZADÁNÍ

Diplomant bere na vědomí, že je povinen vypracovat diplomovou práci samostatně, bez cizí pomoci, s výjimkou poskytnutých konzultací. Seznam použité literatury, jiných pramenů a jmen konzultantů je třeba uvést v diplomové práci.

Datum převzetí zadání	Podpis studenta

Annotation Sheet

Title:	CFD Modelling of Horizontal Water Film Evaporation
Author:	Bc. Radomír Kalinay
Academic year:	2016/2017
Study program:	Mechanical Engineering
Study field:	Applied Mechanics
Department:	Department of Fluid Dynamics and Thermodynamics
Supervisor:	Ing. Tomáš Hyhlík, Ph.D.

Bibliographical data:	Number of pages	79
	Number of figures	52
	Number of tables	10
	Number of attachments	0

Keywords: convective flow, evaporation, heat and mass transfer, horizontal water film, Computational Fluid Dynamics (CFD), STAR-CCM+, user coding

Abstract: Master's thesis theoretically describes problematics of convective flow and evaporative process and applies numerical approaches related to evaporation of horizontal water film. Based on the review, CFD models are developed and implemented into commercial software STAR-CCM+. Two different developed approaches are validated using the comparison with experimental data.

Název: CFD modelování vypařování z horizontálního vodního filmu

Klíčová slova: konvekce, vypařování, přenos tepla a hmoty, horizontální vodní film, počítačová mechanika tekutin (CFD), STAR-CCM+, uživatelské programování

Anotace: Diplomová práce teoreticky popisuje problematiku přenosu tepla a odpařování vodního filmu. Uvedené a popsané numerické přístupy související s odpařováním horizontálního vodního filmu v rešeršní části, jsou použity pro vytvoření CFD modelů, které jsou implementovány do komerčního softwaru STAR-CCM+. Dva odlišné vytvořené CFD modely jsou validovány prostřednictvím porovnání s experimentálním měřením.

Statement

Hereby I declare that I have written this thesis independently assuming that the results of the thesis can also be used at the discretion of the supervisor of the thesis as its co-author. I also agree with the potential publication of the results of the thesis or its substantial part, provided I will be listed as the co-author.

In Prague, 02 August 2017 …….

Signature

Acknowledgements

I would first like to thank my thesis supervisor Ing. Tomáš Hyhlík, Ph.D. for his advice, remarks and for sharing his experience in related field of expertise with me. Besides my supervisor, I would like to appreciate assistance and support of all who help me to finish this work.

Table of Contents

Table of Figures

List of Tables

Nomenclature

a	Absolute humidity	$\left[\frac{kg}{m^3}\right]$
A	Surface area	$[m^2]$
c_p	Specific heat capacity at constant pressure	$\left[\frac{J}{kg\ K}\right]$
c_V	Specific heat capacity at constant volume	$\left[\frac{J}{kg\ K}\right]$
D_{AB}	Binary mass diffusion coefficient	$\left[\frac{m^2}{s}\right]$
h	Enthalpy	$\left[\frac{kJ}{kg}\right]$
h	Convection heat transfer coefficient	$\left[\frac{W}{m^2\ K}\right]$
h_m	Convection mass transfer coefficient	$\left[\frac{m}{s}\right]$
ΔH^{vap}	Latent heat of vaporisation	$\left[\frac{kJ}{kg}\right]$
j_A	Diffusive mass flux of species relative to the mixture mass average velocity	$\left[\frac{kg}{s\ m^2}\right]$
K	Thermal conductivity	$\left[\frac{W}{m\ K}\right]$
M	Molar mass (molecular weight)	$\left[\frac{kg}{mol}\right]$
$\dot{m}$	Mass flow rate	$\left[\frac{kg}{s}\right]$
$\dot{n_A}$	Mass of species *A* generated per unit volume	$\left[\frac{kg}{s\ m^3}\right]$
p	Pressure	$[Pa]$
$\dot{Q}$	Heat flow/Rate of heat	$[W]$
$\dot{q}$	Rate of energy generation per unit volume	$\left[\frac{W}{m^3}\right]$
R	Gas constant	$\left[\frac{J}{K\ mol}\right]$
T	Thermodynamic temperature	$[K]$
t	Temperature	$[°C]$
V	Volume	$[m^3]$
x	Specific humidity	$\left[\frac{kg_V}{kg_A}\right]$

Greek letters

α	Thermal diffusivity	$\left[\frac{m^2}{s}\right]$
α	Absorptivity	$[1]$
β, β_T	Volumetric thermal expansion coefficient	$\left[\frac{1}{K}\right]$
β_ω	Vapour expansion coefficient	$[1]$
ε	Emissivity	$[1]$
θ	Dimensionless temperature	$[1]$
μ	Dynamic viscosity	$[Pa\ s]$
ν	Kinematic viscosity	$\left[\frac{m^2}{s}\right]$
ρ	Reflectivity	$[1]$
ρ	Density	$\left[\frac{kg}{m^3}\right]$
σ	Stefan-Boltzmann constant	$\left[\frac{W}{m^2\ K^4}\right]$
τ	Transmissivity	$[1]$
τ_{ii}	Shear stress	$\left[\frac{N}{mm^2}\right]$
φ	Relative humidity	$[\%]$
ω	Mass fraction	$[1]$

Subscripts and superscripts

", sat	Saturated
∞	Ambient
A	Dry air
atm	Atmospheric
AV	Moist air mixture
cond	Conduction
DP	Dew point

ev	Evaporation
in	Inlet
m	Mass
out	Outlet
S	Surface
V	Water vapour

Dimensionless numbers

Gr	Grashof number
Le	Lewis number
Le_f	Lewis factor
Nu	Nusselt number
Pr	Prandtl number
Ra	Rayleigh number
Re	Reynolds number
Ri	Richardson number
Sc	Schmidt number
Sh	Sherwood number
St	Stanton number

1 Introduction

Evaporation of a fluid film is a common engineering problem influencing many technological and industrial applications. The ability to resolve the evaporative phenomenon impacts design of air conditioning systems or automotive and energy industry application, therefore, development of accurate computational fluid dynamics (CFD) models is desirable.

Although various commercial CFD software offer models able to resolve the evaporative process, its investigation is still topical in the academic field, namely works [1] and [2] published within last sixteen (first mentioned) and eight years (second mentioned).

This thesis is focused on the investigation of convective flow over horizontal water film and its evaporation. Theoretical background of heat and mass transfer is studied and later developed CFD models are described.

In mentioned papers, CFD simulations were conducted in software FLUENT and Open-FOAM. The present thesis is taking advantage of commercial software STAR-CCM+ v11.06.011-R8 (later in text STAR-CCM+), which favours Department of Fluid Dynamics and Thermodynamics of Czech Technical University in Prague in terms of broadening knowledge of CFD software.

Developed CFD models are validated using comparison with experimentally measured data. The experimental side was not part of this work and all experimental data used in this work were measured by Bc. Jakub Devera (CTU in Prague, Faculty of Mechanical Engineering, Department of Fluid Dynamics and Thermodynamics).

1.1 Thesis Goals

Apart from the theoretical review, another requirement is to apply gathered knowledge on the development of CFD models. In thesis are presented two different approaches to CFD modelling of horizontal water film evaporation.

Objectives set for the thesis are as follows:

- Discussion of available models applicable in the field of CFD modelling of horizontal water film evaporation.
- Description of validation experiment and formulation of the problem for the numerical solution. Description of used mathematical models.
- Development of the post-processing like model and the model based on direct application of Fick's law.
- Discussion of an influence of radiation.
- Testing of an influence of used computational mesh.
- Discussion of obtained results and comparison of experimental data.

1.2 Sketch of the Thesis

The first part of the thesis is focused on theoretical background related to the thermodynamics of moist air (chapter 2), heat transfer problematics (chapter 3) and heat and mass transfer analogy (chapter 4). Descriptions of simulated problematics, identification of the flow and review of possible approaches are following (chapter 5).

Thermodynamics of the moist air is described in a way to gather knowledge necessary to understand the evaporative phenomenon. The chapter focused on heat transfer problematics is focused on the description of mechanisms related to the heat transfer and convective heat transfer is reviewed in detail. Heat and mass transfer analogy is investigated since one of the CFD models is based on its principles. Description and identification of the simulated problem are crucial for understanding simulated phenomena.

Next are described developed models from the theoretical side (chapter 6). Implementation of developed models into STAR-CCM+ and their results are then described (chapter 7). Eventually, developed models are compared and results are discussed (chapter 8). Overall summary (chapter 9) is evaluating the accomplishment of thesis objectives.

CFD models are described from the theoretical side to highlight their principles and differences. The description of models implementation into STAR-CCM+ would be helpful in reproducing results of the thesis. Results of developed models are compared and discussed in order to evaluate their validity and utilisation. Furthermore, advantages and disadvantages of CFD models are mentioned.

2 Thermodynamics of Moist Air

In this chapter thermodynamics of moist air is presented. An only homogeneous mixture of moist air is reviewed since the heterogeneous mixtures are not relevant to this work. A homogeneous mixture of moist air might be characterised as a mixture of dry air and water in gaseous state – water vapour [3].

2.1 Fundamental Properties of Moist Air

For common engineering calculations, it is sufficient to assume the gas mixture as an *ideal gas*. *Equation of state* which relates pressure, temperature and density of a substance might be written as follows

$$pV = RT \;\; or \;\; p = \rho RT \,. \tag{2.1}$$

Gas constant R in equation (2.1) is determined for particular gas from relation

$$R = \frac{R_u}{M}, \tag{2.2}$$

where R_u is the *universal gas constant,* which value is 8.314 [J/mol K], and *M* is the *molar mass (molecular weight)*.

Differences of real dry air parameters from those determined via equation of state of an ideal gas are small. In the case of temperature range from 200 to 500 K and pressure range from 0.1 to 1 MPa is the difference less than 3%. Deviation for water vapour is even smaller for pressure less than 1 kPa. [4]

For mixture of ideal gases is applicable *Dalton's law* – "*total pressure of mixture is equal to the sum of partial pressures of components"* [3]

$$p_{mixture} = \sum_i p_i \,. \tag{2.3}$$

The assumption of Dalton's law simplifies the issue of determining thermodynamic properties of moist air.

Temperature and pressure are dependent properties for pure substances during phase-change processes, and there is the one-to-one correspondence between temperature and pressure. At a given pressure the temperature at which a pure substance changes phase is called the saturation temperature T_{sat}. Likewise, at a given temperature, the pressure at which a pure substance changes phase is called the saturation pressure p_{sat}.

It should be strictly distinguished difference between *saturated pressure* and *partial pressure*. Saturated pressure p_{sat} of a pure substance is defined as *the pressure exerted by its*

vapour in phase equilibrium with its liquid at a given temperature [5]. Partial pressure p_V is defined as *the pressure of a gas or vapour in a mixture with other gases* [5]. For example, atmospheric air a mixture of dry air and water vapour, and atmospheric pressure is the sum of the partial pressure of dry air and the partial pressure of water vapour.

The rate of evaporation from open water bodies such as lakes is controlled by the difference between saturated vapour pressure at water temperature and the partial pressure of water vapour. For example, the saturated vapour pressure of water at 20°C is 2.34 kPa. Therefore, a bucket of water at 20°C left in a room with dry air at 101 325 Pa and 20°C will continue evaporating until one of two things happens: the water evaporates away (there is not enough water to establish phase equilibrium in the room), or the evaporation stops when the partial pressure of the water vapour in the room rises to 2.34 kPa at which point phase equilibrium is established. [5]

By relation (2.2) might be determined the gas constants of dry air R_A and water vapour R_V. For a given *specific humidity x,* the gas constant is

$$R_{AV} = \frac{R_A + x\,R_V}{1 + x}. \tag{2.4}$$

Gas constant of a moist air might be of course also defined based on *relative humidity φ*

$$R_{AV} = R_A\left(1 + 0.378\,\varphi\frac{p_V^{"}}{p}\right), \tag{2.5}$$

where *p* is *absolute pressure* and $p_V^{"}$ is *saturated vapour pressure* for a given temperature. [4]

From combination of Dalton's law and state equation, it is possible to determine the density of moist air as [4]

$$\rho_{AV} = \rho_A + \rho_V = \rho_A(p) - \frac{1.317\,10^{-3}p_V^{"}}{T}\varphi\,, \tag{2.6}$$

however, in this work was adopted following equation to determine the density of moist air [6]

$$\rho = \frac{p}{RT}\frac{M_A(1+x)}{\left(1 + \frac{M_A}{M_V}x\right)}, \tag{2.7}$$

because of easier application into STAR-CCM+.

2.2 Moist Air Humidity

To determine the total amount of water vapour in moist air mixture, parameter denoted as *humidity* is used. The amount of water vapour in the moist air might be different and generally is distinguished as:

- *Unsaturated* – partial pressure of water vapour is smaller than saturated water vapour for identical temperature
- *Saturated* – partial pressure of water vapour is equal to saturated water vapour for identical temperature
- *Oversaturated/Supersaturated* – saturated air containing additional water in liquid or solid state

Humidity is determined in different ways:

Absolute humidity *a* - Weight of water vapour in a volume of 1 m^3 moist air. Units are [kg/m^3] and it is called also as *water vapour density* ρ_V for a given pressure of water vapour p_V and temperature *T*. The range of the absolute humidity is $a \in < 0, \rho_V^{"}(T) >$. It is measured directly by absorption of water vapour in volume of air of exact dimensions and collected water is then weighted.

Partial pressure of water vapour p_V - It is related to absolute humidity through state equation. When air pressure remains constant then partial pressure of water vapour remain same in case of temperature change.

Relative humidity *φ* - Measurable property. States how much is the moist air saturated; maximum value is 100%. The dry air of particular temperature and pressure can contain only a limited amount of water vapour. When this amount is exceeded, water vapour condensates [7]. The higher the temperature and pressure are, the higher is the maximum potential amount of water vapour. For $\varphi = 100\%$ is the air saturated. Considering atmospheric air surrounding us, the pressure changes are small and it might be said that the relative humidity is dependent on temperature and the amount of water vapour in the air. Relative humidity is defined as follows

$$\varphi = \frac{\rho_V}{\rho_V^{"}} = \frac{p_V}{p_V^{"}}, \tag{2.8}$$

where $\rho_V^{"}$ is density of saturated water vapour.

Specific humidity *x* - Derived property. States amount of mass of water vapour (in g or kg) to the unity of mass (in g or kg) of dry air. Specific humidity is derived as follows

$$x = \frac{m_V}{m_A} = \frac{V\,\rho_V}{V\,\rho_A} = \frac{R_A\,p_V}{R_V\,p_A} = \frac{M_V}{M_A}\,\frac{p_V}{p - p_V} = 0.622\,\frac{\varphi p_V^{"}}{p - \varphi p_V^{"}}. \tag{2.9}$$

From above-mentioned quantities, are *specific* and *relative humidity* most often used in engineering design, therefore it is suitable to mention formula defining inverse relation to (2.9)

$$\varphi = \frac{p}{p_V^{"}} \frac{x}{0.622 + x}. \tag{2.10}$$

Overall it should be kept in mind that for *higher temperatures the potential amount of water vapour in moist air mixture is greater*.

Temperature of dew point T_{DP} – Temperature, for which becomes the moist air saturated during isobaric cooling. Condensed droplets will occur on the surface of an object of dew point temperature if we assume object's interface with moist air. For dew point temperature applies relation

$$p_V = p_V^{"}(T_{DP}) . \tag{2.11}$$

2.3 Moist Air Enthalpy

In thermodynamics, the amount of heat contained in one kilogramme of substance is called *enthalpy h*. The difference of enthalpy of the initial and final state is characterised as the amount of heat/energy needed for state change for one kilogramme of substance. [8]

When dealing with moist air problem it is common to determine enthalpy for one kilogramme of dry air which contains *x* kg of water vapour. Enthalpy of 1+x kg mixture is then [4]

$$h_{1+x} = h_A + x\, h_V . \tag{2.12}$$

To determine the enthalpy of dry air, the formula is [4]

$$h_A = c_p\, t , \tag{2.13}$$

where c_p is *specific heat capacity at constant pressure*. Enthalpy of water vapour is calculated according to following relation [4]

$$h_V = 1.01\, t + (2\,500 + 1.84\, t)\, x . \tag{2.14}$$

After examination of (2.13), it should be noted that zero enthalpy is given to the air of zero temperature. In the case of the moist air enthalpy, the dependency is given by *temperature* and *pressure*. It is so, that for constant temperature and increasing pressure enthalpy is decreasing.

3 Heat Transfer Theory

Based on our everyday experience, we know that a cold object in a warmer surrounding gets warmer and inversely hot object gets colder in the cold surrounding. This phenomenon and so the science related is denoted as *heat transfer*. Heat transfer deals with basic principles of thermodynamics and it is more widening its knowledge.

Heat transfer science is based on the equilibrium of heat between two systems. Heat is a form of energy that can be transferred from one system to another, as result of temperature difference [7].

Basic principles of thermodynamics needed for heat transfer examination are the *first* and *second law of thermodynamics*. The first law requires that the *rate of energy transferred into a system is equal to the rate of increase of the energy of that system*. The second law requires that *heat is transferred in the direction of decreasing temperature*. [9]

The temperature difference is the driving force for heat transfer and that is analogous to the voltage difference for electric current or to pressure difference for fluid flow.

Main mechanisms of heat transfer are *conduction*, *convection* and *radiation*. These mechanisms might undergo simultaneously. Since this work is related mainly to the problem influenced by convection, it is convenient that this mechanism will be described in more details.

3.1 Conduction

Conduction should be assumed as a phenomenon, which undergoes on the *atomic* and *molecular* level. It is likely to be defined as a heat transfer mechanism between more energetic to less energetic particles of a substance due to interactions between the particles. Conduction can take place in *solids*, *liquids* or *gases*. For solids and liquids, molecular interactions are stronger and more frequent due to lattice vibrations. Therefore, heat transfer in solids and liquids is more effective. In the case of assuming conduction in gas, imagine a closed impermeable rectangular volume infinite in length with horizontal boundaries of different temperature. Consider assumption of no bulk motion in this control volume. Molecules will be moving freely along the control volume, because of no lattice, but the presence of temperature gradient will cause energy transfer by conduction and therefore the overall direction of molecules will be from the molecule of higher energy to the molecule of lower energy. [7] [10]

Coming to mechanisms of heat conduction in different phases of substances the heat transfer is realised by:

- *GAS*: molecular collisions and molecular diffusions
- *LIQUID*: molecular collisions and molecular diffusions
- *SOLID*: Lattice vibrations and flow of free electrons

In the case of gas and liquid, the mechanisms are identical. The difference is that liquids exert stronger intermolecular force field.

When determining the rate of heat conduction through solid wall, *Fourier's law of heat conduction* is used

$$\dot{Q}_{cond} = -k\,A\,\frac{dT}{dx}. \tag{3.1}$$

In (3.1) *k* is the *thermal conductivity*, *A* is frontal area and $\frac{dT}{dx}$ is temperature gradient mentioned above. Temperature gradient is the slope of the temperature curve on *T-x diagram* (considering *x* as a direction), in other words, the temperature distribution across the dimension corresponding the change of width of the solid wall. Negative sign in Fourier's law ensures that heat transfer in the positive *x* direction is a positive quantity.

3.1.1 Thermal Conductivity

Consider two mugs of identical geometry (wall thickness mainly) made of different materials: aluminium and stainless steel. Both are filled with the same volume of 90°C water. After a certain amount of time, water in an aluminium mug will be colder than in stainless steel mug. For stainless steel and aluminium, the thermal conductivities *k* are 16 [W/m K] and 205 [W/m K], respectively [11].

The thermal conductivity of a material can be defined as *the rate of heat transfer through a unit thickness of the material per unit area per unit temperature difference*. The thermal conductivity of a material is a measure of the ability of the material to conduct heat. For higher value the heat transfer is more intensive and vice versa.

The kinetic theory of gases predicts and the experiments confirm that the thermal conductivity of gases can be determined as follows

$$k = \frac{\sqrt{T}}{\sqrt{M}}, \tag{3.2}$$

where *T* is the thermodynamic temperature and *M* molar mass [7].

According to [12] thermal conductivity of dry air and water vapour mixture might be determined as follows

$$k_{AV} = \frac{\left(X_A k_A M_A^{0.33} + X_V k_V M_V^{0.33}\right)}{\left(X_A M_A^{0.33} + X_V M_V^{0.33}\right)}, \tag{3.3}$$

where X_A and X_V are

$$X_A = \frac{1}{1 + 1.608\,x} \quad and \quad X_V = \frac{x}{x + 0.622}. \tag{3.4}$$

Figure 1 shows the dependency of thermal conductivity on relative humidity for moist air mixture evaluated according to (3.3). It can be concluded that for increasing relative humidity the thermal conductivity decreases.

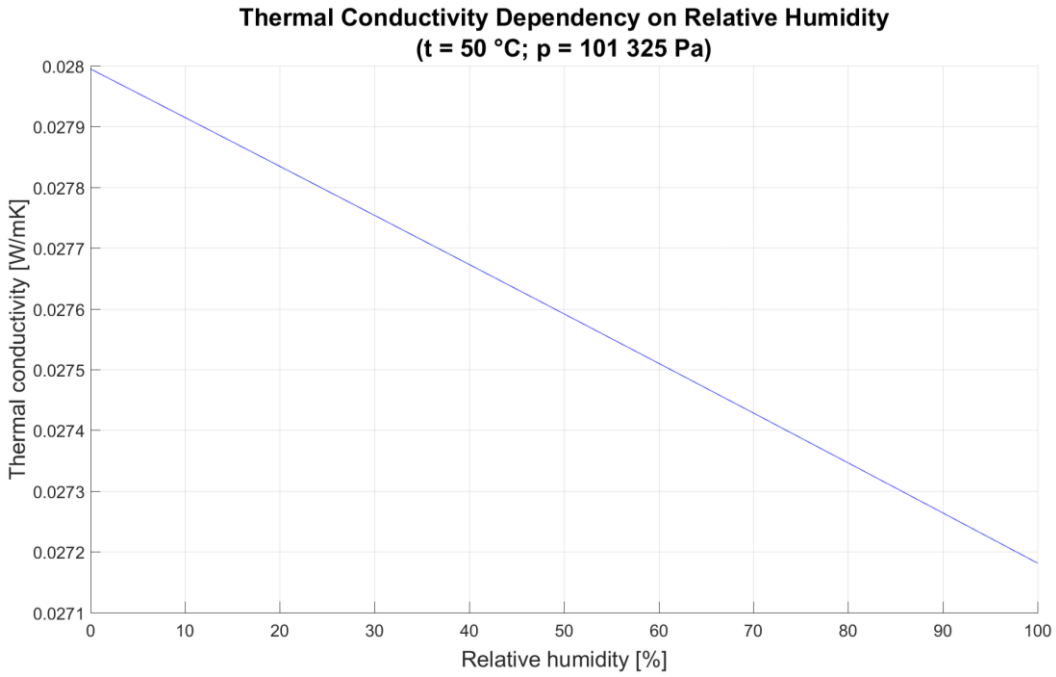

Figure 1 – Thermal conductivity of moist air dependency on relative humidity for constant temperature and pressure.

3.1.2 Thermal Diffusivity

Thermal diffusivity α defines how much the heat diffuses through the material and it is defined as

$$\alpha = \frac{k}{\rho\, c_p}. \tag{3.5}$$

Note that from relation (3.5) can be seen that thermal diffusivity is a ratio of *heat conducted* to *heat stored* in the material. The larger the thermal diffusivity, the faster the propagation of heat into the medium. A small value of thermal diffusivity means that heat is mostly absorbed by the material and a small amount of heat is conducted further. [7]

Since this work is related to moist air problematics, Figure 2 displays thermal diffusivity dependency on relative humidity. From this figure, might be concluded that with increasing humidity the thermal diffusivity is decreasing. In other words, in the case of 100% relative humidity heat is more stored in the substance than conducted further.

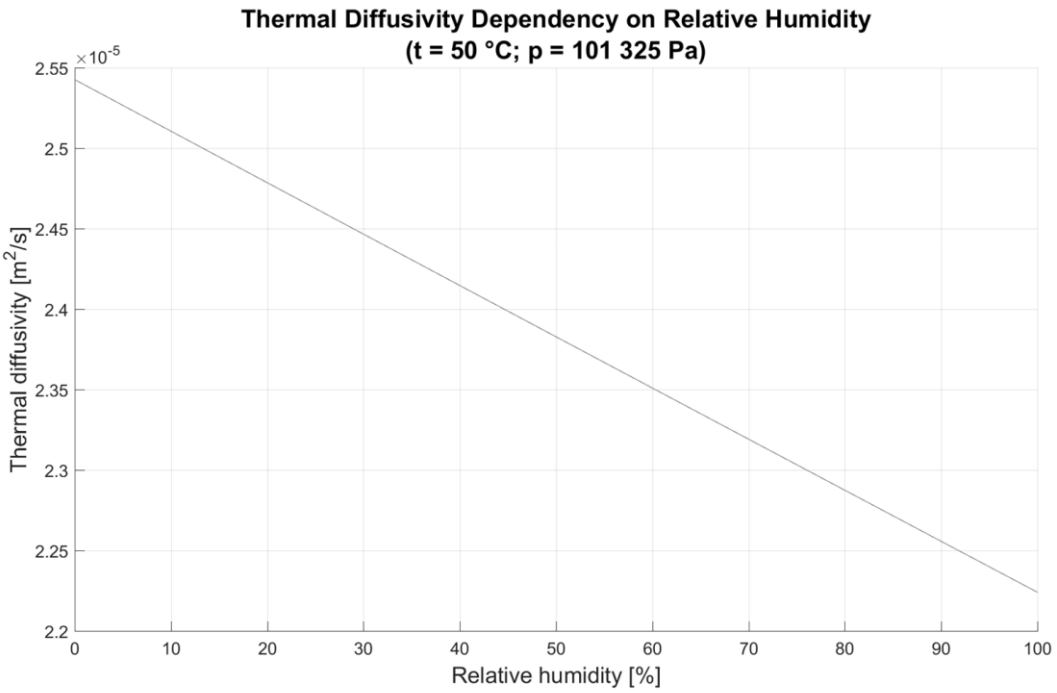

Figure 2 – Thermal diffusivity of moist air dependency on relative humidity for constant temperature and pressure.

3.2 Radiation

Radiation is the energy emitted by matter in the form of electromagnetic waves (or photons) as a result of the changes in the electronic configurations of the atoms or molecules. Unlike conduction and convection, the transfer by radiation does not require the presence of an intervening medium. In this chapter, the radiation will be assumed constant for all wavelengths at a given temperature.

Radiation is a volumetric phenomenon, and all solids, liquids, and gases emit, absorb, or transmit radiation to varying degrees. However, radiation is usually considered to be a surface phenomenon for solids that are opaque to thermal radiation such as metals, wood, and rocks since the radiation emitted by the interior regions of such material can never reach the surface and the radiation incident on such bodies is usually absorbed within a few microns from the surface. [7]

Maximum heat emitted by radiation is determined by the *Stefan-Boltzmann law* as [10]

$$\dot{Q_{max}} = \sigma \, A_S \, T_S^4 \, , \tag{3.6}$$

where σ = 5.670 10^{-8} [W/m^2 K^4] is the Stefan-Boltzmann constant, A_S surface of object, T_S thermodynamic temperature of the object. In (3.6) the maximum heat rate is determined for idealized black body, for nonidealized objects radiation rate is determined as [7]

$$\dot{Q_{max}} = \varepsilon \, \sigma \, A_S \, T_S^4 \, . \tag{3.7}$$

In (3.7) there is the only difference from (3.6) in new parameter *emissivity* ***ε***. Emissivity is radiation property and its maximum value is for a blackbody. The emissivity of a given surface is the *measure of its ability to emit radiation energy in comparison to a black body at the same temperature*, therefore emissivity has value within $\varepsilon \in < 0 ; 1 >$.

Radiation flux incident on a surface is called irradiation and total incident radiation energy is absorbed, reflected or transmitted. Assuming this, there are radiation properties *absorptivity α, reflectivity ρ* and *transmissivity τ* for which follows relation [7]

$$\alpha + \rho + \tau = 1 \,. \tag{3.8}$$

Absorptivity is a property that determines the *fraction of the irradiation absorbed by the surface*. Reflectivity is a property that determines the *fraction of the radiation reflected by the surface*. It should be noted that reflectivity is dependent on the direction of the reflected radiation. Transmissivity is a property that determines the *fraction of the radiation transmitted by the surface*. [10]

Employing *Kirchhoff's Law*, emissivity and absorptivity yields into a relation

$$\varepsilon(T) = \alpha(T) \,, \tag{3.9}$$

that is, *the emissivity of a surface at temperature T is equal to its absorptivity for radiation coming from a blackbody at the same temperature* [7].

Assuming Kirchhoff's Law (3.8) becomes

$$\varepsilon + \rho + \tau = 1 \,, \tag{3.10}$$

which greatly simplifies the radiation analysis and this approach is also adopted in STAR-CCM+.

In the case of solving heat transfer problems by CFD simulations, radiation heat transfer is often neglected. However, one should be cautious with such assumption. When proceeding heat transfer simulation where natural convection is dominant, radiation heat transfer portion is significant [13].

3.3 Convection

Convection is the mode of energy transfer between a solid surface and the adjacent liquid or gas, and it involves the combined effects of conduction and fluid motion. Although the mechanism of diffusion (random motion of fluid molecules) contributes to this transfer, the dominant contribution is generally made by the bulk or gross motion of fluid particles.

When determining heat transfer rate from a heated object *Newton's law of cooling* is employed

$$\dot{Q} = h \, A_S \, (T_S - T_\infty) \,, \tag{3.11}$$

where *h* is the *convection heat transfer coefficient* [W/m^2 K]. Convection heat transfer coefficient *h* is not a property of the quiescent fluid and its determination is quite difficult. It is dependent on *density, viscosity, thermal conductivity, specific heat, surface geometry* and *flow conditions*. Such number of factors influencing the value of convection heat transfer coefficient is given by the fact that it is determined by the boundary layer that develops on the surface. [7] [10]

When dealing with convection two regimes are distinguished – *forced* and *natural convection*. In engineering problems, those two could be assumed as separate, but a situation may arise for which free and forced convection effects are comparable – *mixed convection*. In the following text these three regimes will be described, but first convection transfer equations in boundary layer need to be introduced.

3.3.1 The Forced Convection Transfer Equations in Laminar Boundary Layer Flow

To fully understand the convective phenomenon, boundary layer behaviour will be described. Another motivation to introduce transfer equations in the boundary layer is to present the theoretical background to be able derive the dimensionless numbers relevant to heat and mass transfer analysis. This text and following chapters (3.3.1.1, 3.3.2 and 3.3.2.1) is based on literature [10], [7], [14] and [15].

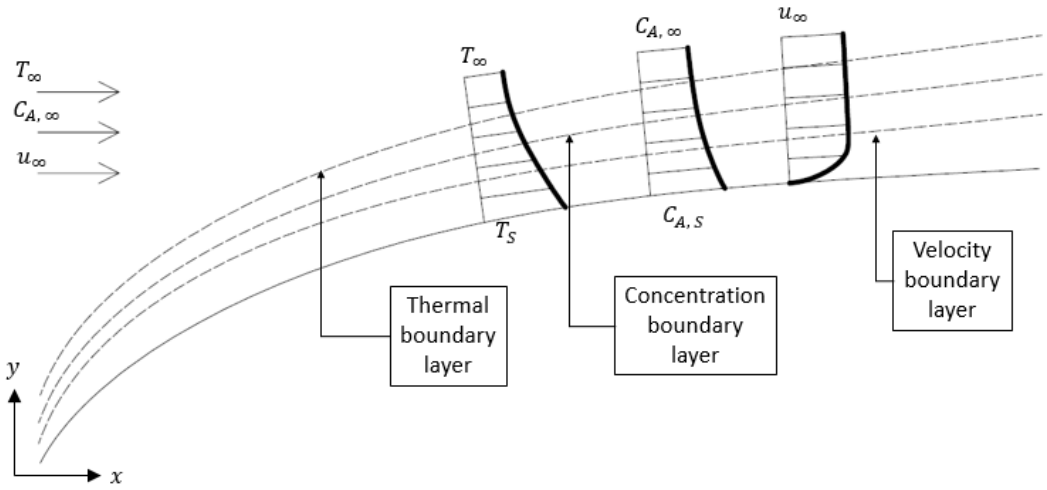

Figure 3 – Thermal, concentration and velocity boundary layers evolution along the surface [10].

Let's assume a fluid film on a surface (Figure 3); it may be observed three types of boundary layers: *velocity*, *thermal* and *concentration*.

In the case of **velocity boundary layer** *conservation law of mass* is relevant; The net rate at which mass enters the control volume must equal zero. Following this and differentiating the mass flow on 2D element (Figure 4) the continuity equation is obtained

$$\frac{\partial(\rho u)}{\partial x} + \frac{\partial(\rho v)}{\partial y} = 0\,. \tag{3.12}$$

Equation (3.12) must be satisfied at every point of the boundary layer and it is applicable for both single and multi-component species fluid.

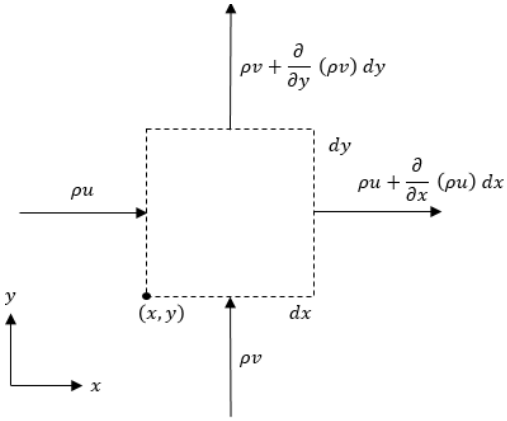

Figure 4 – Differential control volume (2D element) for mass conservation [10].

Another law which needs to be satisfied in the boundary region is Newton's second law of motion; Sum of all forces acting on the control volume must equal the net rate at which the momentum leaves the control volume. Two kinds of forces act on control volume in the boundary layer: *body forces*, proportional to the volume, and *surface forces,* proportional to the area.

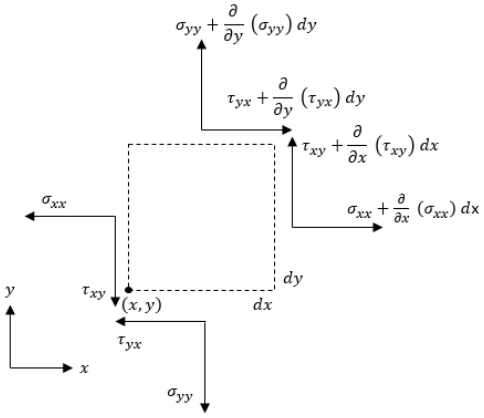

Figure 5 – Normal and shear stresses for a differential control volume (2D element) [10].

Using a Taylor series expansion for the stresses (stresses shown in Figure 5), the net surface force of each two directions may be expressed as

$$F_{Sx} = \left(\frac{\partial \sigma_{xx}}{\partial x} - \frac{\partial p}{\partial x} + \frac{\partial \tau_{yx}}{\partial y}\right) dx\, dy\,, \tag{3.13}$$

$$F_{Sy} = \left(\frac{\partial \tau_{xy}}{\partial x} + \frac{\partial \sigma_{yy}}{\partial y} - \frac{\partial p}{\partial y}\right) dx\, dy\,. \tag{3.14}$$

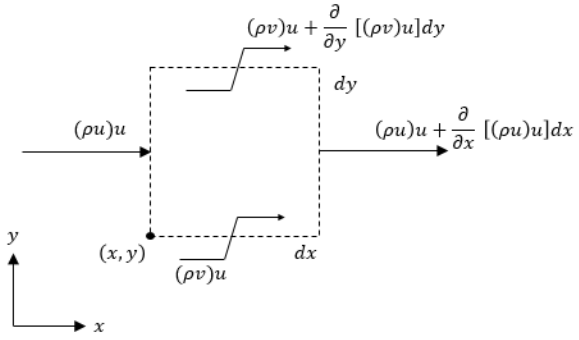

Figure 6 – Momentum fluxes for differential control volume (2D element) [10].

To fulfil Newton's second law evaluation of motion momentum fluxes for the control is missing. After relating momentum fluxes in *x* direction (according to Figure 6), it is obtained

$$\rho\left(u\frac{\partial u}{\partial x}+v\frac{\partial v}{\partial y}\right)=\frac{\partial}{\partial x}(\sigma_{xx}-p)+\frac{\partial \tau_{yx}}{\partial y}+X\,. \tag{3.15}$$

Equation in *y* direction is analogous to (3.15)

$$\rho\left(u\frac{\partial v}{\partial x}+v\frac{\partial v}{\partial y}\right)=\frac{\partial \tau_{xy}}{\partial x}+\frac{\partial}{\partial y}\left(\sigma_{yy}-p\right)+Y\,. \tag{3.16}$$

Normal and shear stresses in equations (3.15) and (3.16), where *X* and *Y* are *body forces*, might be substituted according to [16]. From the boundary layer theory, it might be assumed that velocity component in *x* direction is much larger than in *y* direction, and gradients normal to the surface are much larger than those along the surface. Therefore, in case of momentum equation, normal stresses are negligible and shear stress reduce to

$$\tau_{xy}=\ \tau_{yx}=\mu\left(\frac{\partial u}{\partial y}\right). \tag{3.17}$$

Considering foregoing, the overall continuity equation (3.12) and *x*-momentum equation (3.15) reduce to

$$\frac{\partial u}{\partial x}+\frac{\partial v}{\partial y}=0\,, \tag{3.18}$$

$$u\frac{\partial u}{\partial x}+v\frac{\partial u}{\partial y}=\ -\frac{1}{\rho}\frac{\partial p}{\partial x}+v\frac{\partial^2 u}{\partial y^2}\,, \tag{3.19}$$

and *y*-momentum equation to

$$\frac{\partial p}{\partial y}=0\,. \tag{3.20}$$

Equations (3.19) and (3.20) follows another simplifications and approximations – incompressible flow and negligible body forces.

When applying energy conservation requirement to the control volume in the **thermal boundary layer** (Figure 7), following physical processes are considered:

a) *advection* of thermal and kinetic energy
b) energy transferred via *molecular processes* (*conduction* mainly)
c) energy transferred by *work* interactions involving *body* and *surface forces*

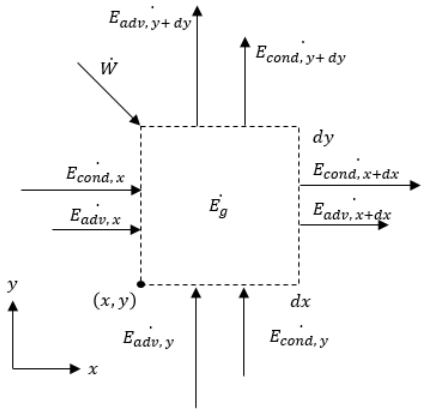

Figure 7 – Differential control volume (2D element) for energy conservation [10].

After balancing energy fluxes transferred via processes listed above, the *thermal energy equation* is obtained for the control volume

$$\rho u\frac{\partial e}{\partial x}+\rho v\frac{\partial e}{\partial y}=\frac{\partial}{\partial x}\left(k\frac{\partial T}{\partial x}\right)+\frac{\partial}{\partial y}\left(k\frac{\partial T}{\partial y}\right)-p\left(\frac{\partial u}{\partial x}+\frac{\partial v}{\partial y}\right)+\mu\Phi+\dot{q}\,, \tag{3.21}$$

where the term $p\left(\frac{\partial u}{\partial x}+\frac{\partial v}{\partial y}\right)$ represents a reversible conversion between kinetic and thermal energy and $\mu\Phi$ the *viscous dissipation*.

It is more common to work with a formulation based on the fluid enthalpy *h*, rather than its internal energy *u*. Therefore, the relation of enthalpy and internal energy is introduced

$$h=u+\frac{p}{\rho}. \tag{3.22}$$

After assumption that the substance is *ideal gas,* $dh=c_p\,dT$, *incompressible,* $c_v=c_p$ and $du=c_v\,dT=c_p\,dT$, the thermal energy equation reduces to

$$\rho c_p\left(u\frac{\partial T}{\partial x}+v\frac{\partial T}{\partial y}\right)=\frac{\partial}{\partial x}\left(k\frac{\partial T}{\partial x}\right)+\frac{\partial}{\partial y}\left(k\frac{\partial T}{\partial y}\right)+\mu\Phi+\dot{q}\,. \tag{3.23}$$

Further simplification is possible based on assumption that temperature gradient in *y* direction is much larger than in *x* direction and the mixture has constant properties $(k,\mu,\text{etc.})$. The energy equation then reduces to

$$u\frac{\partial T}{\partial x}+v\frac{\partial T}{\partial y}=\alpha\ \frac{\partial^2 T}{\partial y^2}+\frac{\nu}{c_p}\left(\frac{\partial u}{\partial y}\right)^2 . \tag{3.24}$$

Since the binary mixture with species concentration gradients is assumed, the governing equation for **concentration boundary layer** needs to be resolved. Processes which affect the transport of species in a differential control volume (Figure 8) in the boundary layer are *advection* (motion driven by mean velocity of the fluid), *diffusion* (motion relative to the mean motion) and *chemical reactions.*

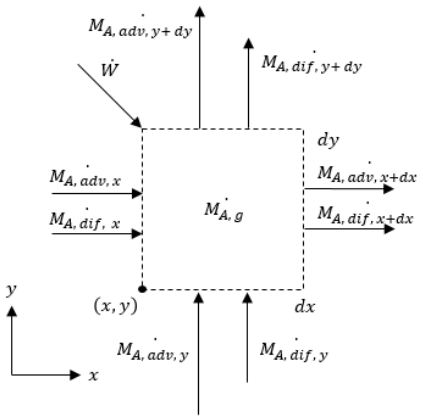

Figure 8 – Differential control volume (2D element) for species conservation [10].

The net rate at which species *A* enters the control volume due to the advection in the *x* direction is

$$\begin{aligned}\dot{M}_{A,\ adv,\ x}-\dot{M}_{A,\ adv,\ x+dx}&=\rho_A u\,dy-\left[(\rho_A u)+\frac{\partial(\rho_A u)}{\partial x}dx\right]dy\\&=-\frac{\partial(\rho_A u)}{\partial x}\,dx\,dy\,.\end{aligned} \tag{3.25}$$

With assumption of *incompressible fluid* and using *Fick's law,* the net rate at which species *A* enter the control volume due to the *diffusion* in *x* direction is

$$\begin{aligned}&\dot{M}_{A,\ diff,\ x}-\dot{M}_{A,\ diff,\ x+dx}=\\&=\left(-\frac{D_{AB}\partial\rho_A}{\partial x}\right)dy-\left[\left(-D_{AB}\frac{\partial\rho_A}{\partial x}\right)+\frac{\partial}{\partial x}\left(-D_{AB}\frac{\partial\rho_A}{\partial x}\right)dx\right]dy=\\&=\frac{\partial}{\partial x}\left(D_{AB}\frac{\partial\rho_A}{\partial x}\right)dx\,dy\,.\end{aligned} \tag{3.26}$$

Balancing the species conservation of control volume (according to Figure 8), *species continuity equation* is obtained (assuming ρ constant)

$$u\frac{\partial\rho_A}{\partial x}+v\frac{\partial\rho_A}{\partial y}=\frac{\partial}{\partial x}\left(D_{AB}\frac{\partial\rho_A}{\partial x}\right)+\frac{\partial}{\partial y}\left(D_{AB}\frac{\partial\rho_A}{\partial y}\right)+\dot{n_A}\,, \tag{3.27}$$

where $\dot{n}_A$ is the mass of species *A* generated per unit volume due to chemical reactions $\left[\frac{kg}{s\,m^3}\right]$. Also in case of concentration boundary layer, it is so, that the gradient normal to the surface is much larger than in direction along the surface. After assumptions that the mixture is *non-reacting* and that the boundary layer properties $(k, \mu, c_p \text{ etc.})$ are of species *B* the species continuity equation is

$$u\frac{\partial C_A}{\partial x} + v\frac{\partial C_A}{\partial y} = D_{AB}\frac{\partial^2 C_A}{\partial y^2}. \tag{3.28}$$

Equations (3.18), (3.19), (3.24) and (3.28) may be solved to determine the spatial variations of *u*, *v*, *T* and C_A. For incompressible, constant property flow *continuity* and *x-momentum equations* are uncoupled from *energy equation* and *species conservation equation*. That means *continuity* and *x-momentum equations* may be solved for the velocity field *u(x, y)* and *v(x, y)* without consideration of *energy* and *species conservation* equations [10]. On the other hand, the *energy* and *species conservation* equations are *coupled* to the velocity field, that arises in a condition, that firstly the velocity field needs to be calculated to obtain temperature and concentration fields.

After resolved temperature and concentration fields heat and mass coefficients, respectively, might be determined. These coefficients are strongly dependent on velocity field, therefore, it is desirable to do not underestimate the process of exact identification of the convective regime.

Equations (3.18), (3.19), (3.24) and (3.28) in foregoing text are stated for that case of zero normal velocity. This might be applicable only for cases, where there is no simultaneous heat and mass transfer. When considering the mass transfer, normal velocity component *v* cannot be assumed as zero and *continuity, momentum, energy* and *species conservation* equations need to be in *general* form. These equations might be characterised by advection terms on the left-hand side and a diffusion term on the right-hand side. Such forms characterise *low-speed*, ***forced convection flows***. Equations characterising the ***natural convection flow*** will be described in 3.3.2.

Although boundary layer equations are stated under certain simplifications and approximation, they are described well enough to be able to identify key boundary layer parameters, as well as analogies between momentum, heat and mass transfer.

3.3.1.1 Non-dimensionalizing Forced Convection Boundary Layer Equations

In this chapter, the boundary layer equations will be non-dimensionalize. A similar approach might be found in the literature [7], [10], [16]. To normalise governing equations derived in 3.3.1, flow variables need to be in dimensionless form. Let's start with the *independent variables*

$$x^* = \frac{x}{L} \quad and \quad y^* = \frac{y}{L}, \tag{3.29}$$

where *L* is a characteristic length of the surface of interest – in the case of the horizontal plate, *L* would be the length of the horizontal plate. *Dependent dimensionless variables* are

$$u^* = \frac{u}{V} \quad and \quad y^* = \frac{v}{V}, \tag{3.30}$$

where *V* is arbitrary *reference velocity*. Other variables are defined as follows

$$T^* = \frac{T - T_S}{T_\infty - T_S} \quad and \quad C_A^* = \frac{C_A - C_{A,S}}{C_{A,\infty} - C_{A,S}} \quad and \quad p^* = \frac{p}{\rho V^2}. \tag{3.31}$$

After substituting relations (3.29) to (3.31) into conservation equations introduced in chapter 3.3.1, the complete set of equations of boundary layer equations becomes

$$\frac{\partial u^*}{\partial x^*} + \frac{\partial v^*}{\partial y^*} = 0, \tag{3.32}$$

$$u^* \frac{\partial u^*}{\partial x^*} + v^* \frac{\partial u^*}{\partial y^*} = -\frac{dp^*}{dx^*} + \frac{1}{Re_L} \frac{\partial^2 u^*}{\partial y^{*2}}, \tag{3.33}$$

$$u^* \frac{\partial T^*}{\partial x^*} + v^* \frac{\partial T^*}{\partial y^*} = \frac{1}{Re_L Pr} \frac{\partial^2 T^*}{\partial y^{*2}}, \tag{3.34}$$

$$u^* \frac{\partial C_A^*}{\partial x^*} + v^* \frac{\partial C_A^*}{\partial y^*} = \frac{1}{Re_L Sc} \frac{\partial^2 C_A^*}{\partial y^{*2}}. \tag{3.35}$$

In equations (3.32) to (3.35) were introduced following *dimensionless numbers*

$$Re = \frac{vL}{\nu} \quad and \quad Pr = \frac{\nu}{\alpha} \quad and \quad Sc = \frac{\nu}{D_{AB}}, \tag{3.36}$$

where Re is *Reynolds number* defining the *ratio of inertia and viscous forces*, *Pr* is *Prandtl number* defining *ratio of momentum and thermal diffusivities*, *Sc* is *Schmidt number* defining *ratio of momentum and mass diffusivities* [14], [10].

3.3.2 The Natural Convection Transfer Equations in Laminar Boundary Layer Flow

Similar approach as for forced convection - the conservation of mass and energy equations - is also applicable for natural convection. Inertia and viscous forces remain important, as does energy transfer by *advection* and *diffusion*, however, the main difference is a strong contribution of *buoyancy forces* in case of natural convection force [7], [10].

Let's assume a vertical hot plate immersed in a quiescent fluid body (Figure 9). The natural convection flow is assumed to be steady, laminar and two-dimensional, and the fluid to be Newtonian with constant properties, including density, with one exception: the density difference $\rho - \rho_\infty$ is to be considered, since it is this density difference between the inside and the outside of the boundary layer that gives rise to buoyancy force and sustains flow – this is known as the *Boussinesq approximation***.** [7]

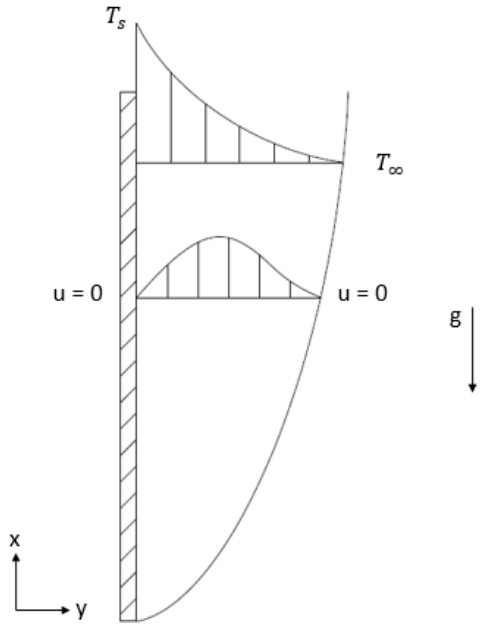

Figure 9 - Velocity and temperature profiles for natural convection flow over a hot vertical plate [7].

Forces influencing differential volume element of the flow are shown in Figure 10**,** assuming Newton's second law $\delta m\, a = F$ and substituting for acceleration *a* and forces *F* it is obtained *x*-momentum equation

$$\rho\left(u\frac{\partial u}{\partial x} + v\frac{\partial u}{\partial y}\right) = \mu\frac{\partial^2 u}{\partial y^2} - \frac{\partial P}{\partial x} - \rho g\,. \tag{3.37}$$

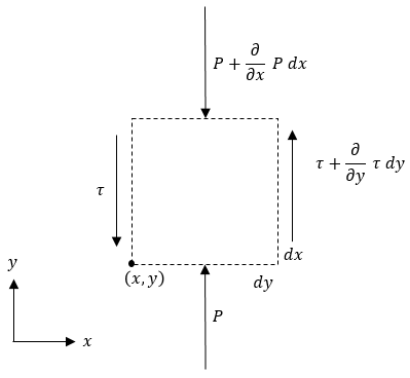

Figure 10 – Forces acting on a differential volume element (2D element) in the natural convection [7].

Introducing the relation for the variation of hydrostatic pressure in a quiescent fluid $\frac{\partial P}{\partial x} = -\rho_\infty g$, the *x*-momentum equation might be rewritten in the form

$$\rho\left(u\frac{\partial u}{\partial x}+v\frac{\partial u}{\partial y}\right)=\mu\frac{\partial^2 u}{\partial y^2}-(\rho-\rho_\infty)g\,. \tag{3.38}$$

Recalling the definition of *volume expansion coefficient* β, expression $\rho-\rho_\infty$ might be substituted as $\rho\beta(T-T_\infty)$; applying foregoing and dividing both sides by ρ, *x*-momentum equation becomes

$$u\frac{\partial u}{\partial x}+v\frac{\partial u}{\partial y}=\nu\frac{\partial^2 u}{\partial y^2}+g\beta(T-T_\infty)\,. \tag{3.39}$$

Equation (3.39) and two following give complete set of equations governing the flow of natural convection

$$\frac{\partial u}{\partial x}+\frac{\partial v}{\partial y}=0\,, \tag{3.40}$$

$$u\frac{\partial T}{\partial x}+v\frac{\partial T}{\partial y}=\alpha\frac{\partial^2 T}{\partial y^2}\,. \tag{3.41}$$

It should be noted that in energy equation (3.41) viscous dissipation was neglected due to small velocities which are associated with natural convection [10].

In the case of natural convection momentum equation involves temperature and thus momentum and energy equations are coupled and need to be solved simultaneously [7], [10].

3.3.2.1 Non-dimensionalizing Natural Convection Boundary Layer Equations

In order to non-dimensionalize *x*-momentum and energy equation, all dependent and independent variables need to be dimensionless. This might be achieved similarly as it is in chapter 3.3.1.1

$$x^*=\frac{x}{L}\;,\;\; y^*=\frac{y}{L}\;,\;\; u^*=\frac{u}{V}\;,\;\; v^*=\frac{v}{V}\;,\;\; T^*=\frac{T-T_\infty}{T_s-T_\infty}, \tag{3.42}$$

where *L* is the characteristic length and *V* is the arbitrary reference velocity. After introducing dimensionless variables equations (3.39) and (3.41) will become

$$u^*\frac{\partial u^*}{\partial x^*}+v^*\frac{\partial u^*}{\partial y^*}=\frac{g\beta(T_S-T_\infty)L}{V^2}T^*+\frac{1}{Re}\frac{\partial^2 u^*}{\partial y^{*2}}, \tag{3.43}$$

$$u^*\frac{\partial T^*}{\partial x^*}+v^*\frac{\partial T^*}{\partial y^*}=\frac{1}{Re\;Pr}\frac{\partial^2 T^*}{\partial y^{*2}}\,. \tag{3.44}$$

The dimensionless product on the right side of the equation (3.43) is a direct consequence of the buoyancy force – *Grashof number Gr*. Since the reference velocity *V* is arbitrary, it is convenient to work with alternative form that is obtained by multiplying by $Re^2 = \left(\frac{VL}{\nu}\right)^2$

$$Gr = \frac{g\beta(T_s - T_\infty)L}{V^2}\left(\frac{VL}{\nu}\right)^2 = \frac{g\beta(T_S - T_\infty)L^3}{\nu^2}. \tag{3.45}$$

The Grashof number plays the same role in natural convection as Reynolds number in forced convection; Grashof number represents the *ratio of the buoyancy force to the viscous force* acting on the fluid. But on the other hand, to distinguish laminar and turbulent regime *Rayleigh number Ra* is used, which is defined as $Ra = Gr\ Pr$ [7]. According to [17] the transition from laminar to turbulent regime for horizontal plates is at Rayleigh number $Ra_L \approx 10^7$.

3.3.3 Forced and Natural Convection Difference

The main difference when examining the natural and forced convection was already mentioned in 3.3.2; *In the case of natural convection the contribution of buoyant forces cannot be neglected which is reflected when momentum equation is derived*.

In engineering, there might be rarely observed problems influenced by only forced or natural convection. It is so that these two types of flow are *superposed* and product of $\frac{Gr}{Re^2}$, called *Richardson number*, is used to distinguish their relation as follows [7], [10]:

- $\frac{Gr}{Re^2} \approx 1$ - effects of forced and natural convection is comparable
  - $Nu = f(Re, Gr, Pr)$
- $\frac{Gr}{Re^2} \ll 1$ - natural convection effects might be neglected
  - $Nu = f(Re, Pr)$
- $\frac{Gr}{Re^2} \gg 1$ - forced convection effects might be neglected
  - $Nu = f(Gr, Pr)$

Above is pointed out how the evaluation of *Nusselt number Nu* differs in different types of forced and natural convection flows combinations. To evaluate the Nuselt number exactly is very important because Nusselt number is used to determine the *heat transfer coefficient h* ($Nu = \frac{hL}{k_f}$).

4 Heat and Mass Transfer Analogy

4.1 Diffusive Mass Transfer

Since similar physical mechanisms are associated with heat and mass transfer diffusion, it is not surprising that the corresponding rate equations are of the same form. Whereas for heat transfer the rate of diffusion is described by *Fourier's law,* for mass transfer it is *Fick's law* which defines the transfer of species *A* in a binary mixture of *A* and *B* as follows [10]

$$\mathbf{j}_A = -\rho D_{AB} \nabla \omega_A \,, \tag{4.1}$$

where j_A represents the mass flux of species *A*, i. e. it is the amount of *A* that is transferred per unit time and per unit area perpendicular to the direction of transfer, and it is proportional to the mixture density $\rho = \rho_A + \rho_B$ and to the gradient in the species mass fraction $\omega_A = \rho_A/\rho$.

From (4.1) might be concluded that the evaluation of mass transfer is strongly dependent on transport property, namely, *binary diffusion coefficient* or *mass diffusivity* D_{AB}. Evaluation of *binary diffusion coefficient* should not be underestimated and it is recommended to review literature [18] to achieve correct results.

4.2 Convective Mass Transfer

When assuming the mass transfer from a wetted surface the driving force is the concentration gradient. For fully developed concentration boundary layer the mass flow rate of species *A* may be computed from an expression of the form

$$\dot{m}_A = h_m \, A_s \left(\rho_{A,s} - \rho_{A,\infty}\right), \tag{4.2}$$

where $\rho_{A,s}$ is the density near the surface, $\rho_{A,\infty}$ is the reference density and h_m is the *mass transfer coefficient*. Form of (4.2) is analogous to Newton's law of cooling.

Mass transfer may be evaluated involving the *Sherwood number* Sh as follows [15]

$$Sh = \frac{h_m L}{D_{AB}}. \tag{4.3}$$

Sherwood number Sh in (4.3) is defined as *dimensionless concentration gradient at the surface, therefore,* it might be said that Sherwood number and Nusselt number are analogous since the Nusselt number is defined as *dimensionless temperature gradient at the surface*. As it is for Nusselt and Sherwood numbers, same analogy is applicable to *Prandtl number* and *Schmidt number*. Prandtl number defines the *ratio of the momentum and thermal diffusivities* and Schmidt number *ration of momentum and mass diffusivities.* Since such analogies are employed the heat transfer *h* and mass transfer h_m coefficients may be related as [10]

$$\frac{h}{h_m} = \frac{k}{D_{AB} Le^n} = \rho c_p Le^{1-n} . \tag{4.4}$$

In (4.4) the *Lewis number Le* is used, which defines *ratio of the thermal and mass diffusivities* [15] [10]

$$Le = \frac{\alpha}{D_{AB}} = \frac{Sc}{Pr} . \tag{4.5}$$

5 Problem Specification and Approaches Review of CFD Models

One of the main goals of this thesis is to present a solution how to model convective flow and evaporative phenomenon using a commercial CFD tool. From the point of view of CFD simulation, mentioned problems were investigated on test case based on experimental measurements. In following chapters is described experimental test rig, on which was based simulation model, and flow conditions are identified. After that is presented a review of possible approaches of simulating investigated phenomena.

All experimental data used in this thesis were measured and provided by Bc. Jakub Devera (CTU in Prague, Faculty of Mechanical Engineering, Department of Fluid Dynamics and Thermodynamics), experimental measurements were not part of this work.

5.1 Problem Specification

The examined phenomena, convective flow over horizontal water film and its evaporation, have been measured on a test rig. Since experimental side was not a part of this work, the description of the test rig will not go into details.

The test rig is constructed of inlet nozzle directing the incoming air. After the nozzle, there is a rectangular duct of 0.09 m^2 cross-sectional area. On the bottom of the rectangular duct is located a fluid film of width *W* and length *L*. Rectangular duct ends with a contraction connected to an outlet pipe. The flow rate of entering air is controlled by a small fan located near the end of the outlet pipe. Figure 11 shows design drawing of the test rig. In Figure 12 might be seen the model of the computational domain used for simulation.

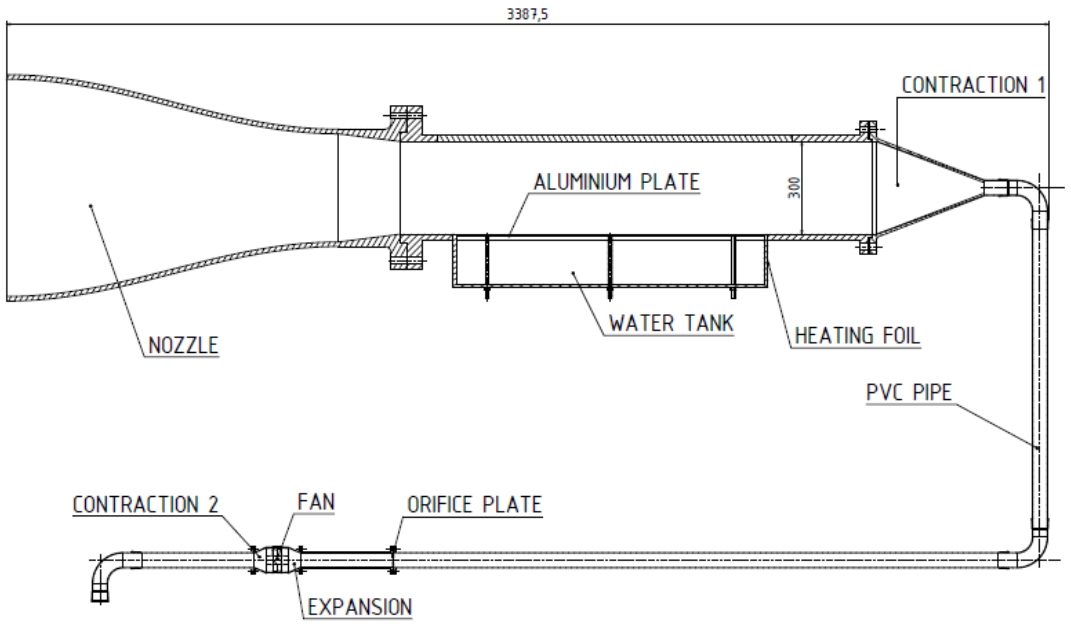

Figure 11 - Design drawing of the test rig (Credit: Image courtesy of Bc. Jakub Devera, CTU in Prague, Faculty of Mechanical Engineering, Department of Fluid Dynamics and Thermodynamics).

Inlet mass flow rate is kept at a constant value to achieve approximately 0.1 m/s velocity in the mixing area. Inlet air has properties of ambient, i. e. inlet temperature and humidity are given and not regulated. Heating of the fluid film, which is located at the bottom of the mixing area, is provided by the heated aluminium plate and during measurement the fluid film is maintained at constant temperature. The height of water film might be assumed as constant because of water tank below. A mixture of air and water vapour is then carried through the contraction and outlet pipe outwards in such a way to do not influence conditions of the inlet ambient air.

Figure 12 – CFD 3D model of the test rig.

5.1.1 Identification of Flow

The experiment described in 5.1 which is simulated, might be categorised as a problem of internal flow over a horizontal plate. When assuming reference properties, those of ambient conditions and heated fluid film are assumed.

The product of $\frac{Gr}{Re^2}$ is evaluated to distinguish whether the forced or natural convection is dominant. In case of ambient conditions given during measurements conducted during July 2016 the $\frac{Gr}{Re^2} > 65$, based on 3.3.3 the *natural convection is dominant*; however, role of the *forced convection is still assumed* since the conditions of natural and forced convection equality is exceeded by only a factor of 10.

Judging the flow from the perspective of natural convection, value of Rayleigh number $Ra > 10^7$ suggests turbulent regime, recalling 3.3.2.1 . Although, the Reynolds number gives values of laminar flow[1], still it is convenient to consider the flow as turbulent – same approach is adopted in [17].

[1] $Re \approx 6.2\ 10^3$; According to [10] $Re = 10^5$ is a transition from laminar to turbulent regime for horizontal plates.

5.2 Approaches Review of Modelling Convection Flow and Evaporative Phenomenon

From 5.1.1 results that the simulated phenomenon will be mainly influenced by the natural convection. To reflect this in simulation, the variation of the density needs to be considered. Such variation is mostly influenced by temperature differences and by the concentration changes of air and water vapour mixture since the evaporative process is involved and the gravity is considered. Foregoing two requirements might be covered by employing the equation of state which reflects both. Such equation becomes

$$\rho = \frac{p}{RT}\frac{M_A\left(1+\frac{\omega_V}{1-\omega_V}\right)}{\left(1+\frac{M_A}{M_V}\frac{\omega_V}{1-\omega_V}\right)}, \tag{5.1}$$

where ω_V is the mass fraction of the water vapour. In (5.1) the pressure *p* might be treated as constant in case of incompressible flow.

To evaluate the evaporative process, firstly the boundary layer needs to be resolved and then the water vapour mass flux might be determined using the heat and mass transfer analogy. In other words, STAR-CCM+ as a CFD tool might be used to resolve the flow (only temperature and velocity fields) and then equations (4.2), (4.4) and (4.5) might be employed to evaluate the water evaporation rate. However, this approach has its limits since the fluid film is assumed only as a heat source and therefore continuum properties do not change due to the evaporated water vapour.

Another approach of modelling evaporation process is to resolve using CFD both - the flow field and the species transport from the source into the computational domain. Article by Yan, Tsay and Lin [19] is focused on the numerical investigation of laminar steady mixed convection flow between two vertical parallel plates covered with fluid film. Dirichlet boundary condition is defined on the air-fluid interface. To enhance the natural convective flow, Boussinesq approximation is introduced – Gr_T and Gr_M, the *Grashof numbers* for *heat* and *mass transfer*, respectively, are implemented in axial-momentum equation. A similar approach might be seen in work of Laaroussi, Lauriat and Desrayaud [1], where commercial solver FLUENT 6.3 was used to conduct the numerical solution and source terms were introduced in the cells adjacent to the walls for the mass (mixture and species) conservation equations to account for vaporisation of the liquid film. This work compares two approaches how to invoke the solutal and thermal buoyancy forces of natural convection flow – *first*, using the Boussinesq approximation, *second*, density variation with changing temperature and water vapour mass fraction. It is important to note that in work of Laaroussi et al. [1] might be seen that for higher interfacial mass fraction the *Richardson* Ri_M ($Ri_M = \frac{Gr_M}{Re^2}$) and *Grashof* Gr_M numbers are increased.

Work of Sosnowski, Petronio and Armenio [2] uses a similar approach as in [19] and [1]; on the air-fluid film interface the Dirichlet boundary condition is defined and the Boussinesq approximation reflecting both, solutal and thermal buoyancy effects, is implemented into the incompressible form of Navier-Stokes equation. Numerical analysis is conducted using Open-

FOAM. The change of the thickness of the fluid film in time is evaluated using the velocity of evaporation and condensation.

Concluding foregoing, two possible approaches how to simulate convection flow and evaporation process will be investigated and adopted in this work. First approach, denoted as *Fick's law Model*, is based on literature [19], [1] and [2], where solutal and thermal buoyancy effects are implemented into momentum equations and the air-fluid film interface is defined as a Dirichlet boundary condition and evaporation rate will be monitored by boundary species flux field function which is based on the theory of Fick's law. The second approach, denoted as *Post-processing Models*, is based on resolving the convective flow and via post-processing, using the heat and mass transfer theory, is evaluated the water evaporation rate.

6 Developed Models

6.1 Fick's Law Model

In this chapter, the Fick's Law Model will be described from the theoretical side. In 7.2 the implementation of this model into STAR-CCM+ will be presented.

6.1.1 Buoyancy Force Source

In the case of the double diffusion problem, the solutal and thermal buoyancy forces can be modelled via the Boussinesq approximation. In [1] the *buoyancy parameter N* is defined invoking thermal and solutal Grashof numbers Gr_T and Gr_M, respectively

$$N = \frac{Gr_M}{Gr_T} = \frac{\beta_\omega (m_{V,S} - m_{A,0})}{\beta_T (T_S - T_0)}, \tag{6.1}$$

where

$$\beta_T = \frac{1}{T_0} \quad and \quad \beta_\omega = \frac{M_A}{M_V} - 1\,. \tag{6.2}$$

Based on eqn. (6.1) might be derived the density variation ρ', which is then implemented into the Navier-Stokes equation [2]

$$\rho' = -\beta_T (T - T_0) - \beta_\omega (\omega - \omega_0)\,. \tag{6.3}$$

In STAR-CCM+ the momentum equation in integral form is [13]

$$\begin{aligned} \frac{\partial}{\partial t}\left(\int_V \rho \chi v\right) dV + \oint_A \rho v \otimes \left(v - v_g\right) \cdot da \\ = -\oint_A pI \cdot da + \oint_A T \cdot da \\ + \int_V \left(f_r + f_g + f_p + f_u + f_\omega + f_L\right) dV\,. \end{aligned} \tag{6.4}$$

To explain the meaning of each member of eqn. (6.4) is out of the scope of this thesis and the nomenclature might be seen in [13]. However, a special attention will be given to the *body force vector due to gravity* f_g. Considering (6.3) f_g might be specified as follows

$$f_g = \rho g \left[\beta_T \left(T_{ref} - T\right) + \beta_\omega \left(\omega_{ref} - \omega\right)\right], \tag{6.5}$$

where are ρ density, T temperature, T_{ref} the reference temperature, $\omega = \frac{m_V}{(m_A+m_V)}$ the vapour mass fraction (m_V and m_A are masses of vapour and air, respectively) and $\omega_{ref} = \frac{m_{V,0}}{(m_{A,0}+m_{V,0})}$ the reference vapour mass fraction. In the form of (6.5) the *body force vector* f_g might be implemented into the STAR-CCM+ segregated solver as a *momentum source*.

6.1.2 Air-Fluid Film Interface Definition

The air-fluid film interface definition is treated similarly as in [19] and [2]. From the theory of evaporation, it is assumed a thin saturated layer of moist air above a fluid film, in which moist air and a liquid film are in thermodynamic equilibrium in this layer. The interfacial concentration of water vapour can be evaluated as follows [2]

$$\omega_V = \frac{M_V}{M_A} \frac{p_V^{"}\,\varphi}{p_{atm} - p_V^{"}\,\varphi\,\left(1 - \frac{M_V}{M_A}\right)}, \tag{6.6}$$

where $p_V^{"}$ is the saturated pressure of water vapour and p_{atm} the atmospheric pressure. M_V and M_A are the molar masses of vapour and air, respectively. φ is the relative humidity, which equals unity at the air-water film interface. The saturated pressure $p_V^{"}$ [Pa] might be determined as in [2]

$$p_V^{"} = 611.85 \exp\left(17.502\,\frac{T_s - 273.15}{T_s - 32.25}\right), \tag{6.7}$$

where T_s is the temperature of the surface of the water film. Equation (6.7) is a derived form of Tetens Equation.

Above mentioned (6.6) might be derived from expression determining the water vapour mass fraction

$$\omega = \frac{x}{1+x}, \tag{6.8}$$

specific humidity is derived according to (2.9) and its general form is

$$x = \frac{M_V}{M_A} \frac{\varphi p_V^{"}}{p - \varphi p_V^{"}}, \tag{6.9}$$

after combining (6.8) and (6.9), equation (6.6) is obtained.

In STAR-CCM+ the water vapour mass fraction determined by (6.6) is used to define a *species source* on the area of the fluid film to invoke the evaporative process.

6.1.3 Water Evaporation Rate Evaluation

STAR-CCM+ offers activation of field function *Boundary Species Flux*. This field function is resolved via *species transport equation*, which is described in details in STAR-CCM+ User Guide [13]. *Diffusion term* of *species transport equation* is dependent on *diffusion flux* which is related to Fick's law. It should be also noted that the diffusion flux is evaluated with respect to laminar and turbulent diffusion. Since the main interest is in evaporation rate of water vapour relative to the surface of the water film, field function *Boundary Species Flux* is multiplied by water film surface A_S, after that, it is obtained the water evaporation rate $\dot{m_{ev}}$ [kg/s].

6.2 Post-processing Models

Post-processing Models used in this work are divided into two sub-approaches – *Heat Transfer Analogy Based Model* and *Lewis Factor Analogy Based Model*. However, both are based on the concept described in 5.2 and use the STAR-CCM+ as a tool to resolve the flow.

Main characteristics of Post-processing Models is that the continuum in the computational domain is assumed as single-component gas.

6.2.1 Heat Transfer Analogy Based Model

Recalling the equation (4.2) gives an apparatus to evaluate the water evaporation rate. The heat transfer coefficient h_m might be evaluated according to (4.4), where the only variable unknown is the Lewis number *Le*.

For gas mixtures both *Pr* and *Sc* are of the order of magnitude of unity, therefore assuming $Le = 1$ [15] is acceptable. Such assumption simplifies the evaluation of mass transfer coefficient based on the heat transfer coefficient and from (4.4) is derived

$$h_m = \frac{h}{\rho c_p}. \tag{6.10}$$

The heat transfer coefficient *h* is resolved by STAR-CCM+, therefore the equation (4.2) to evaluate the evaporation rate becomes

$$\dot{m}_v = \frac{h}{\overline{\rho_A}\, c_p}\, A_s \left(\rho_{A,s} - \rho_{A,\infty}\right), \tag{6.11}$$

where $\overline{\rho_A}$ is calculated as average density of air near the fluid film and free stream air

$$\overline{\rho_A} = \frac{\rho_{A,S} + \rho_{A,\infty}}{2}, \tag{6.12}$$

specific heat capacity at constant pressure c_p as

$$c_p = \omega_A(T_\infty)\, c_{p,A}(T_\infty) + \omega_V(T_\infty)\, c_{p,V}(T_\infty)\,, \tag{6.13}$$

the density of saturated air near the surface $\rho_{A,S}$ as

$$\rho_{A,S} = \omega_V(T_S)\, \rho_{AV}(T_S)\,, \tag{6.14}$$

the density of ambient air $\rho_{A,\infty}$ of ambient humidity as

$$\rho_{A,\infty} = \omega_V(T_\infty)\, \rho_{AV}(T_\infty)\,. \tag{6.15}$$

In (6.14) and (6.15) is needed to evaluate the density of the moist air based on temperature $\rho_{AV}(T)$. This might be achieved using (5.1).

6.2.2 Lewis Factor Analogy Based Model

Lewis factor Le_f gives an indication of the relative rates of heat and mass transfer in an evaporative process. It is equal to the ratio of the *heat transfer Stanton number St* and to the *mass transfer Stanton number* St_m [20]. *Heat transfer Stanton number St* is defined as a modified Nusselt number and Nusselt number can be assumed as a dimensionless heat flux [10], [20]. Analogical description might be used in case of *mass transfer Stanton number* St_m with *Sherwood number Sh* employed, which is referred as a dimensionless mass flux.

From the definition, Stanton numbers for heat and mass transfer are, respectively, [20]

$$St = \frac{Nu}{Re\ Pr} = \frac{h}{\rho u c_p} \quad and \quad St_m = \frac{Sh}{Re\ Sc} = \frac{h_m}{\rho u}, \tag{6.16}$$

the Lewis factor Le_f is than [20]

$$Le_f = \frac{St}{St_m} = \frac{h}{c_p h_m}\,. \tag{6.17}$$

For air-water vapour mixtures is possible to assume $Le_f = 1$ [20].

Similarly, as in 6.2.1 equation (4.2) is used to evaluate the evaporative rate. Employing (6.17) equation (4.2) becomes

$$\dot{m_v} = \frac{h}{c_p Le_f}\, A_S \left(\rho_{A,s} - \rho_{A,\infty}\right). \tag{6.18}$$

It should be noted, that in [20] the mass transfer coefficient h_m is of units $\left[\frac{kg}{m^2 s}\right]$, and this thesis adopted mass transfer coefficient h_m of units $\left[\frac{m}{s}\right]$, therefore convenient units conversion needs to be undertaken.

In the case of Lewis Factor Analogy Based Model, evaluation of parameters of equation (6.18) is analogical to determining parameters of equation (6.11). However, the evaluation of free stream temperature is different. In the case of Heat Transfer Analogy Based Model the ambient temperature is taken from the boundary condition, but for Lewis Factor Analogy based Model is used an average temperature of a control volume.

Figure 13 shows control volume, which is of width *W* and length *L*, these correspond to width and length of the fluid film area. Height *h* of control volume equals to $h = \frac{x}{H} = 0.67$, this height provides most accurate results.

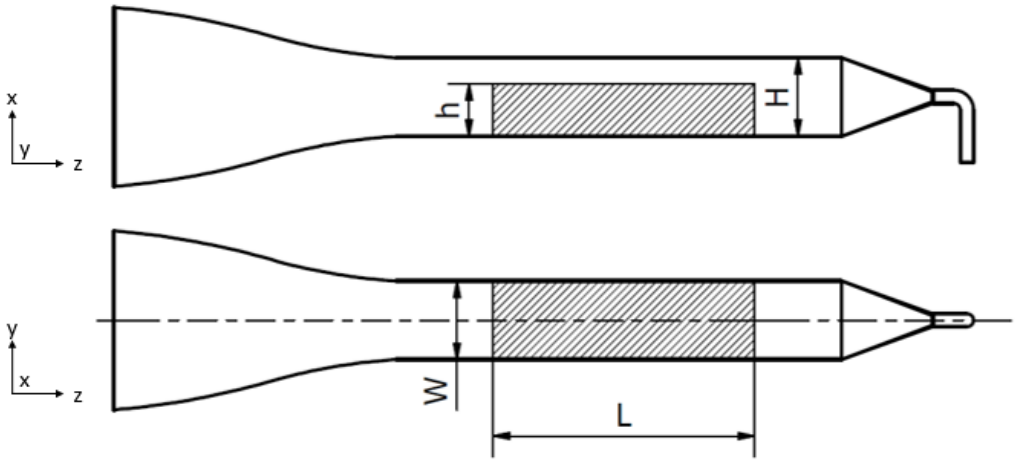

Figure 13 – Dimensions and location of the control volume.

7 Implementation of Developed Models and Results

7.1 General Approach

Chapters 7.1.1 to 7.1.7 describe settings of simulations which are valid for both approaches – Fick's Law Model and Post-Processing Models. Settings which are different for Fick's Law Model and Post-processing Models are presented in 7.2 and 7.3, respectively.

7.1.1 Simulation Setting

Simulations were conducted as three dimensional with gravity effect considered. The continuum is assumed as non-reacting.

Segregated flow model invokes segregated solver which solves momentum equation for each dimension. The linkage between the momentum and continuity equations is achieved with the predictor-corrector approach. Such formulation can be described as using a collocated variable arrangement (opposed to staggered) and Rhie-and-Chow type pressure-velocity coupling combined with a SIMPLE type algorithm. This model is more suitable for constant density flows but it can handle mildly compressible flows and low Rayleigh number natural convection. [13]

Although, the simulated process is a combination of free and forced convection the solution might be assumed as steady. The flow is modelled as turbulent recalling the identification in 5.1.1. *Realisable k-ε Two-Layer model* is selected since it is possible to activate *Buoyancy Driven Two-Layer Type model* correlating the turbulence parameters (turbulent kinetic energy *k* and turbulent dissipation rate ε) for flows where buoyancy forces dominate.

Radiation effect is not neglected due to its significance to temperature field distribution. Since dry air and moist air do not participate in radiation heat transfer the *Surface-to-Surface model* is selected. Radiation properties of surfaces are considered same for all wavelengths, the *Gray Thermal Radiation model* is used, and their values are defined according to [21].

Other settings of simulations are different for each investigated approaches and will be described separately in 7.2 and 7.3.

7.1.2 Convergence

Convergence was assessed based on the *level of residual drop*, *monitoring outlet values* and *water evaporation rate*. Residuals decrease below 10^{-3} is assumed as satisfactory and by monitoring outlet values and water evaporation rate is confirmed that the solution reached steady state solution.

7.1.3 Radiation Influence

In 7.1.1 is stated that radiation is not neglected due to its significance to temperature field distribution. For purpose of this work, this assumption was confirmed by comparing temperature fields of simulations with and without radiation of identical conditions - Figure 14 and Figure 15 respectively. Titles of Figure 14, Figure 15 and Figure 16 suggest type of particular regime and boundary conditions, those terms are explained in 7.1.5.

The result of the comparison can be seen in Figure 16, from which might be concluded that the temperature field of simulation with radiation is significantly warmer. Apart the effect of warmer temperature field should be noted that the character of temperature field is different when the radiation is not considered – top area of the temperature field is significantly colder. Later in the text are shown experimentally measured data (Figure 28, Figure 31, Figure 34, Figure 42, Figure 45 and Figure 48) which confirms that the top area is influenced by the radiative heat transfer.

7.1.4 Mesh Generation

Mesh was created using available meshers in STAR-CCM+. Polyhedral cells were chosen since they provide a balanced solution for complex mesh generation problems and polyhedral mesh contains approximately five times fewer cells than tetrahedral mesh [13].

Prism layers were created in order to accurately simulate the boundary layer. For heat transfer involved problems might be a definition of boundary layer crucial. Volume mesh above the water film is refined to enhance better accuracy.

For both models different meshes were used. The setting of each of them is described in 7.2.1 and 7.3.1.

7.1.5 Boundary Conditions

Figure 17 describes parts of the computational domain and Table 1 how boundary conditions are defined within the computational domain.

Table 1 – Definition of boundary conditions.

Part of the computational domain	Boundary condition definition
• **Inlet**	Mass flow inlet
• **Walls**	Non-adiabatic walls
• **Fluid film**	Wall of static temperature (Post-processing Model) / Wall of static temperature and species source (Fick's Law Model)
• **Outlet**	Pressure outlet

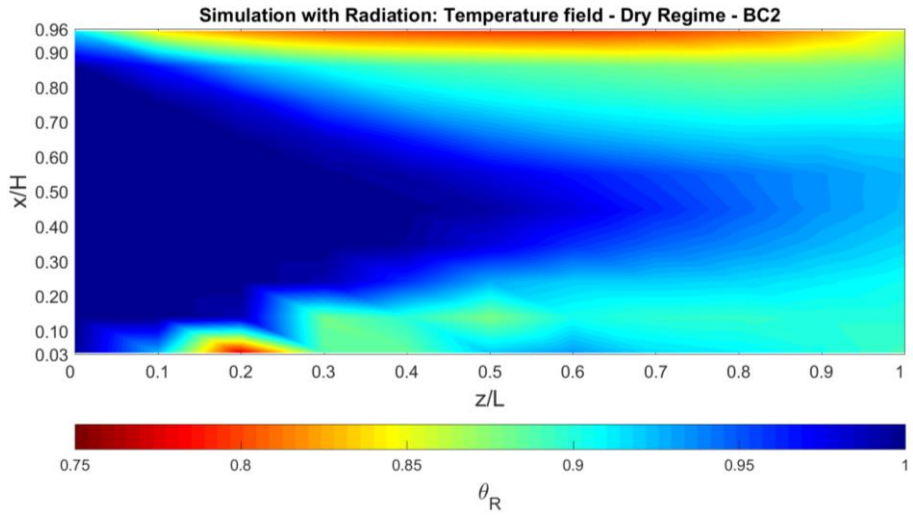

Figure 14 – Temperature field of simulation with radiation for boundary conditions BC2 (Post-processing Models).

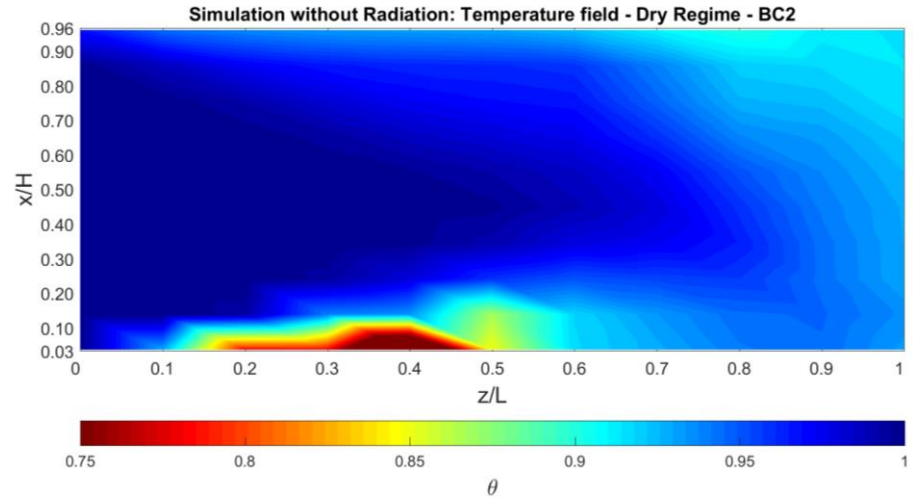

Figure 15 - Temperature field of simulation without radiation for boundary conditions BC2 (Post-processing Models).

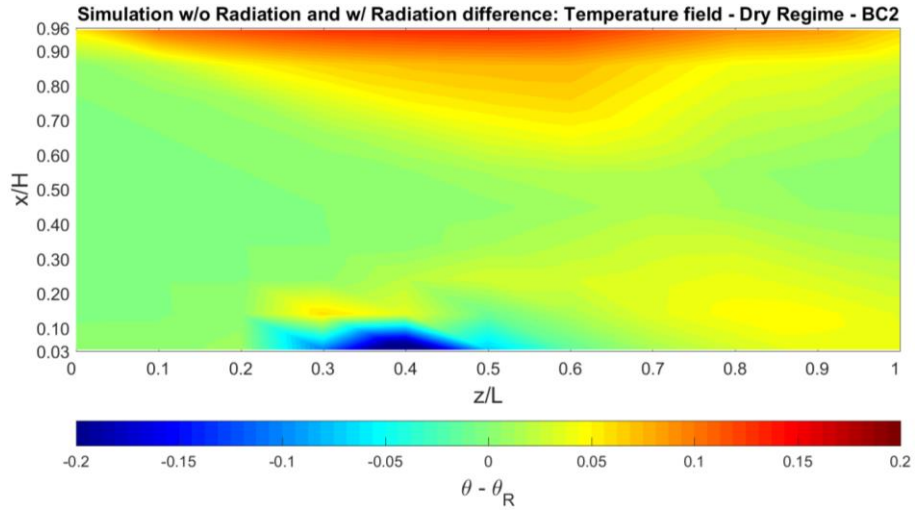

Figure 16 – Simulation with and without radiation temperature field difference for boundary condition BC2 (Post-processing Models).

As it is stated in Table 1 a heat transfer through walls is considered. The test rig is manufactured from different materials; therefore, the heat transfer coefficient distribution is not constant. The distribution of heat transfer coefficient along the test rig shows Figure 18.

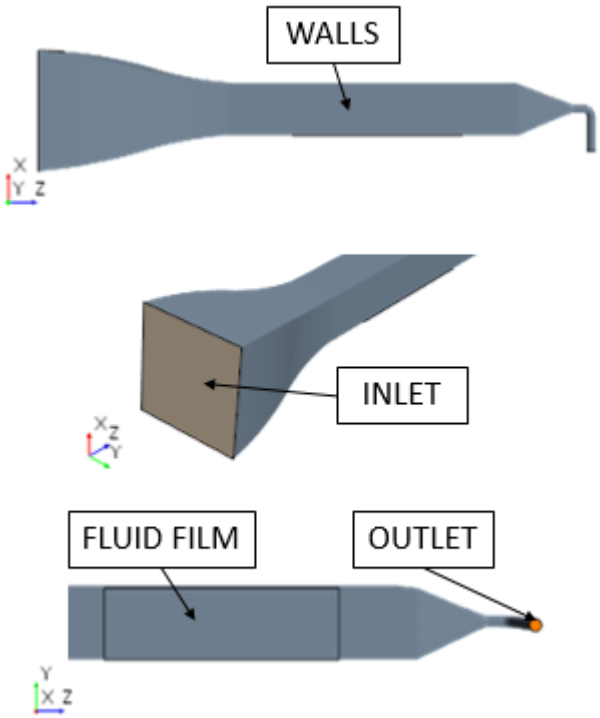

Figure 17 – Parts of the computational domain.

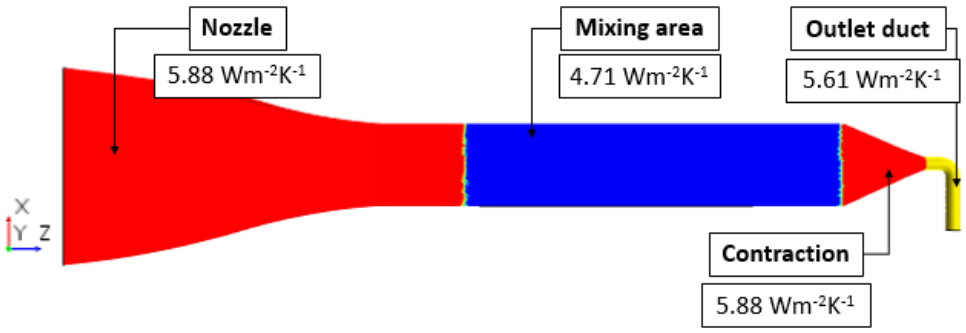

Figure 18 – Heat transfer coefficient along the test rig.

7.1.6 Initialization

Simulations are initialized to ambient conditions. That means properties of a continuum in the domain are for zero iteration same as ambient.

7.1.7 Results Comparison

Simulation results are compared with the experimental measurements from which are the boundary conditions determined. The validity of simulations is confirmed based on a comparison of water evaporation rate, temperature field and outlet temperature in the case of the Post-processing Models. Additionally, the outlet humidity is compared in case of the Fick's Law Model. In the case of Post-processing Models comparing the outlet humidity is not possible since the fluid film is assumed only as a heat source.

Table 2 shows boundary conditions and experimental data for three data sets. These data sets were used to compare simulation results of water evaporation rate, outlet temperature and outlet humidity to experimental data.

Table 2 - Three data sets of experimental data determining boundary conditions for simulations and data used for simulation validity assessment based on water evaporation rate, outlet temperature and outlet humidity comparison.

Parameters / Data set	BC1	BC2	BC3
Boundary conditions			
Reynolds number	6430.72	6290.36	6412.09
Grashof number	4.08E+09	3.26E+09	2.79E+09
Richardson number	98.73	82.49	67.97
Rayleigh number	5.33E+09	4.26E+09	3.65E+09
Prandtl number	1.3061	1.3074	1.3076
Schmidt number	0.4898	0.5086	0.5200
P_{amb} [Pa]	98490	99200	99200
$\omega_{V_{in}}$	0.0134	0.0126	0.0125
$\dot{m}_{in}$ [kg/s]	0.0106	0.0104	0.0106
ΔT [°C]	31.95	25.59	21.89
Experimental data			
θ_{out}	9.43	11.58	13.40
$\omega_{V_{out}}$	0.0255	0.0219	0.0197
$\dot{m}_{ev}/\dot{m}_{in}$ [‰]	12.55	9.47	7.25

The second part of Table 2 are the experimental data. θ_{out} is the outlet dimensionless temperature. Dimensionless temperature is in this work defined as follows

$$\theta = \frac{T - T_S}{T_\infty - T_S}. \tag{7.1}$$

Outlet water vapour mass fraction $\omega_{V_{out}}$ represents the outlet humidity. Water evaporation rate is quantified as a permil of the inlet mass flow rate of the dry air, this relates the evaporative process with the intensity of the inlet flow.

Table 3 and Table 4 shows boundary conditions for simulations used for temperature fields comparison. In Post-processing Models is the water film assumed only as a heat source unlike to the Fick's Law Model, where the fluid film is defined as heat and species source. The same approach was also followed in experimental measurement – two regimes of temperature measurement were proceeded: "dry" and "moist". In the case of dry regime (Table 4), there is only heat transfer considered unlike to moist regime (Table 3), where heat and mass transfer took place simultaneously.

Temperature fields are compared in the centre longitudinal plane of height *H,* which corresponds to the mixing area height, and of length *L*, which corresponds to the fluid film length. In the case of simulation, temperature fields of three planes are averaged to cover the geometrical characteristic of temperature sensors used during experimental measurement. Figure 19 illustrates described approach.

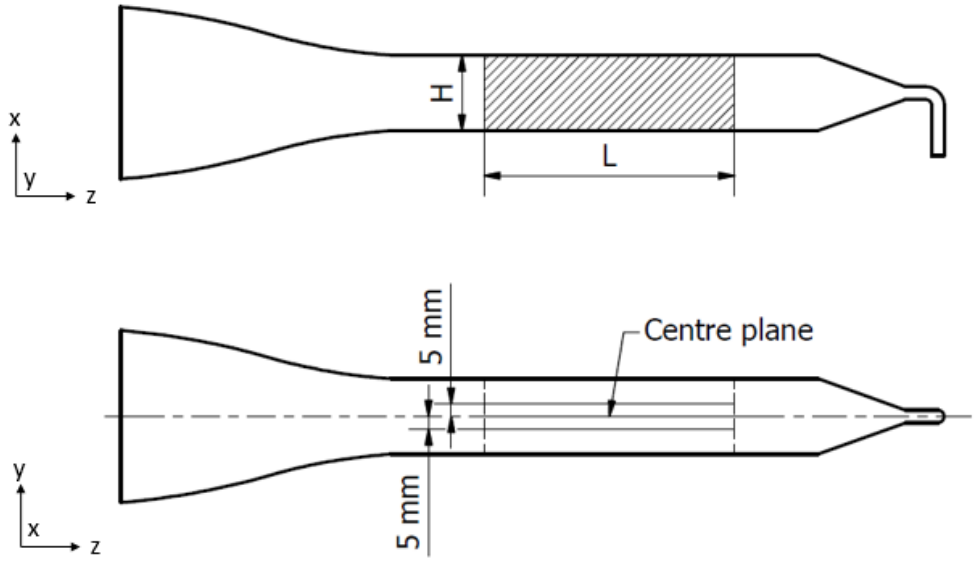

Figure 19 – Position of three longitudinal temperature fields in the simulation.

In tables Table 2, Table 3 and Table 4 are the boundary conditions mostly defined using dimensionless numbers (*Re, Gr, Ri, Ra, Pr* and *Sc*). For *Re* and *Gr* is characteristic length *L* considered as the length of the fluid film. For *Gr* T_s and T_∞ represent water film and ambient temperatures, respectively.

Another parameter used to define boundary conditions is ambient pressure p_{atm}. Inlet vapour mass fraction $\omega_{V_{in}}$represents the inlet humidity. In STAR-CCM+ the species ratio is defined using the vapour mass fraction, therefore it is convenient to employ its usage instead of specific humidity. $\dot{m_{in}}$ is the inlet mass flow of dry air and ΔT is defined as $\Delta T = T_S - T_\infty$ and represents amount of temperature potential. For all boundary conditions listed in tables Table 2, Table 3 and Table 4 are valid assumptions described in 5.1.1.

Table 3 - Three data sets of experimental data (moist regime) determining boundary conditions for simulations used for simulation validity assessment based temperature field comparison.

Parameters / Data set	BC4	BC5	BC6
Boundary conditions			
Reynolds number	6690.88	6544.46	6549.31
Grashof number	5.46E+09	5.19E+09	6.37E+09
Richardson number	122.04	121.12	148.57
Rayleigh number	7.21E+09	6.84E+09	8.41E+09
Prandtl number	1.3198	1.3188	1.3208
Schmidt number	0.4802	0.4855	0.4687
P_{amb} [Pa]	99790	101000	100000
$\omega_{V_{in}}$	0.0052	0.0057	0.0046
$\dot{m_{in}}$ [kg/s]	0.0108	0.0106	0.0105
ΔT [°C]	36.02	34.13	40.12

Table 4 - Three data sets of experimental data (dry regime) determining boundary conditions for simulations used for simulation validity assessment based on temperature fields comparison.

Parameters / Data set	BC7	BC8	BC9
Boundary conditions			
Reynolds number	6689.15	6603.00	6723.52
Grashof number	5.44E+09	5.26E+09	6.25E+09
Richardson number	121.57	120.66	138.28
Rayleigh number	7.18E+09	7.18E+09	8.26E+09
Prandtl number	1.3198	1.3194	1.3218
Schmidt number	0.4805	0.4841	0.4699
P_{amb} [Pa]	99790	101000	100000
$\omega_{V_{in}}$	0.0052	0.0054	0.0040
$\dot{m_{in}}$ [kg/s]	0.0108	0.0107	0.0108
ΔT [°C]	35.92	34.68	39.75

7.2 Fick's Law Model

Following part (7.2.1 to 7.2.6) is describing the implementation of the Fick's Law Model into STAR-CCM+. Chapter 4.10 describes the Fick's Law Model from the theoretical side, recalling this chapter might be principles of model simplified as:

- The effect of natural convection buoyancy forces is activated using implementation of the Boussinesq approximation into the momentum equation as a momentum source.

Boussinesq approximation considers buoyancy forces caused by temperature and solutal differences.

- Water film is defined as heat and species source, in other words, both, heat and mass transfer is simulated.
- Water evaporation rate is evaluated using the implemented field function of STAR-CCM+.

7.2.1 Mesh Generation

Table 5 lists parameters of the mesh which was generated in STAR-CCM+ and used during validity assessment of Fick's Law Model. Values of other parameters which are not mentioned remain set as default.

Table 5 – Settings of used mesh (Fick's Law Model).

Parameters	Values
• **Base Size**	0.014 m
• **Target Surface Size**	80 % of base size
• **Minimum Surface Size**	10 % of base size
• **Surface Growth Rate**	1.3
• **Number of Prism Layers**	8
• **Prism Layer Stretching**	1.1
• **Prism Layer Total Thickness**	0.038 m
• **Wake Refinement (above fluid film)**	50 % of base size

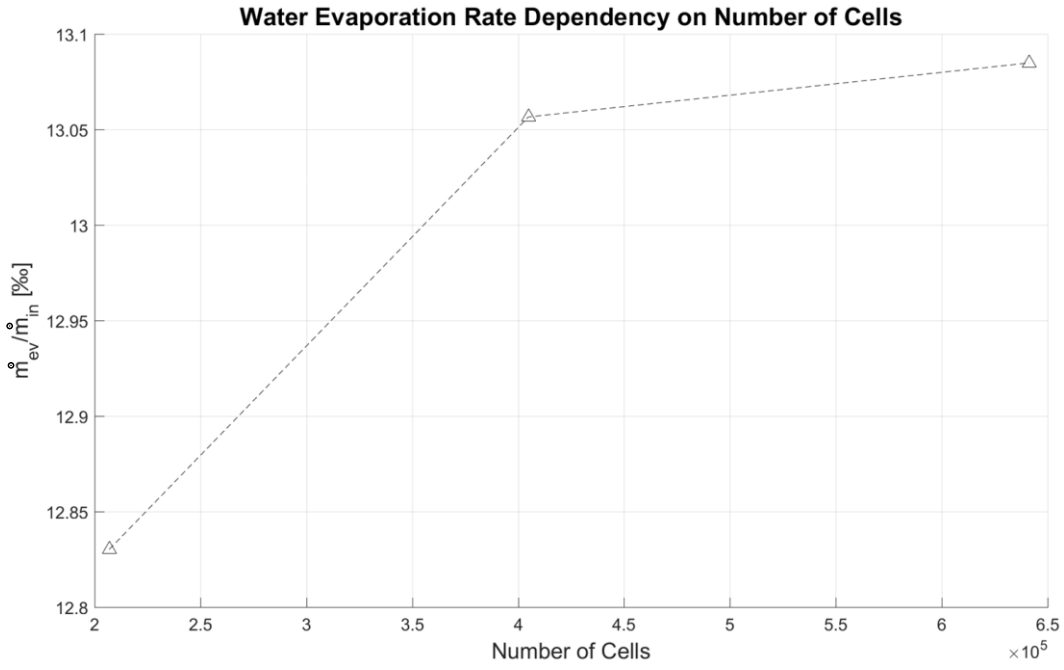

Figure 20 – Water evaporation rate dependency on a number of cells (Fick's Law Model).

The solution mesh dependency test was proceeded. Three meshes with different base size were generated. The dependency of water evaporation rate on a number of cells can be seen in Figure 20, from which results that mesh with 641 349 cells provides efficient convergence.

7.2.2 Boundary Conditions

In the case of Fick's Law Model, the water film area is defined in STAR-CCM+ as a species source and it is considered as an air-water film interface. The water vapour mass fraction on the air-water film interface ω_V is calculated according to (6.6). Temperature on the interface is assumed same as temperature of the plate which is heating up the water film.

To be able to define the species source in STAR-CCM+, equations (6.6) and (6.7) needs to be reproduced using *user defined field functions*. Other boundary conditions are defined according to chapter 7.1.

7.2.3 Simulation Approach

Table 6 describes the simulation setting for Fick's Law Model. *Constant density model* is used as an *Equation of state*. Because of using the constant density model, the Boussinesq approximation needs to be involved to simulate the natural convection.

Table 6 – Simulation setting (Fick's Law Model).

Models	Parameters
• **Three dimensional**	
• **Steady**	
• **Multi-component gas**	Gas Components: H2O, Air
• **Non-reacting**	
• **Segregated flow** (Gradients, Segregated Species)	Convection: 2nd-order (Gradient Method: Hybrid Gauss-LSQ, Limiter Method: Venkatakrishnan, Custom Accuracy Level Selector: 2.0, Verbose: False; Convection: 2nd-order)
• **Constant density**	
• **Turbulent** (Reynolds-Averaged Navier-Stokes)	
• **k-ε Turbulence** (Realizable k-ε Two-Layer, Exact Wall Distance, Two Layer All y+ Treatment, Exact Wall Treatment)	(Convection: 2nd-order, Curvature Correction Option: Off, Two-Layer Type: Buoyancy Driven(Xu))
• **Gravity**	
• **Segregated Fluid Temperature**	Convection: 2nd-order
• **Radiation**	
• **Surface-to-Surface Radiation** (View Factors Calculator)	
• **Gray Thermal Radiation**	Radiation Temperature: 300.0 K

In STAR-CCM+ the Boussinesq model involving the effects of buoyancy force is available. This model covers only temperature differences, though, and it is applicable to single component gas only. Therefore, momentum source corresponding to (6.5) was developed using C programming. Momentum source is treated as *a User coded field function* in STAR-CCM+ and the code might be seen in Appendix A.

Implementation of above mentioned momentum source into STAR-CCM+ does not require any knowledge of C programing language from the user when *User Field Functions* are created according to Table 7.

Table 7 – User field functions definition.

User field functions	Description
• **TRef**	Scalar field function defining the reference temperature [K]. Ambient temperature should be considered as a reference.
• **MwRef**	Scalar field function defining the reference mass fraction of H2O. The ambient mass fraction of H2O should be considered as a reference.

7.2.4 Continuum Definition

Continuum is assumed as a multi-component gas of Air and H2O and related mass fractions define the species ratio.

7.2.5 Convergence

Figure 21 presents residual dependency on iteration in the case of Fick's Law Model. Residuals decrease satisfies convergence requirement defined in 7.1.2.

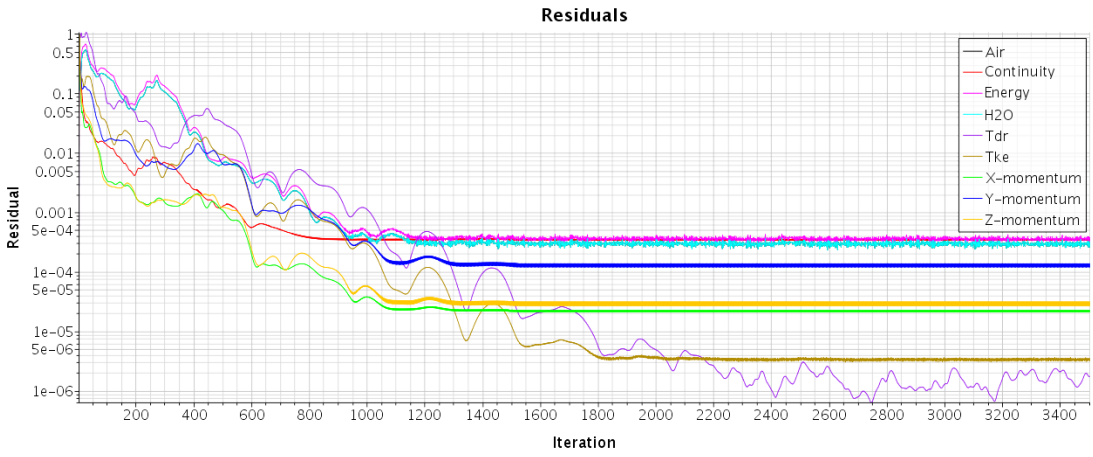

Figure 21 – Residuals dependency on iteration (Fick's Law Model).

Figure 22 shows outlet values and water evaporation rate dependency on iteration, which confirms that simulation reached steady state solution.

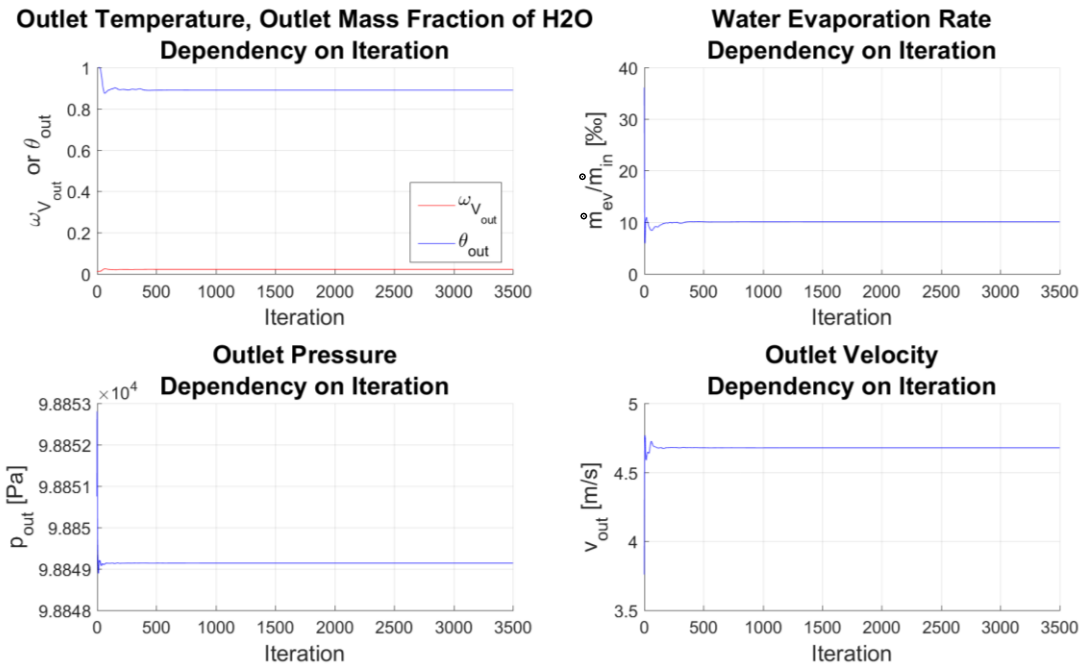

Figure 22 – Monitoring of outlet values and water evaporation rate dependency on iteration (Fick's Law Model).

7.2.6 Results

Dependencies presented in Figure 23, Figure 25 and Figure 26 are within ranges of $\Delta T \in < 20; 34 >$ °C, $\dot{m_{in}} \in < 0.0104;\ 0.0106 >$ and $\omega_{V_{in}} \in < 0.0125;\ 0.0134 >$ assumed as linearly dependent.

From the comparison of experimental data and simulation results of water evaporation rate (Figure 23) might be concluded that the Fick's Law Model deviation from the experiment is within 10%.

Comparison of simulation results and experimental data of outlet humidity dependency on inlet humidity (Figure 25) shows good agreement and simulation results deviation is within the range of 10%.

Simulation results of water evaporation rate and outlet humidity are higher for all boundary conditions compared to the experimental data. This results from the fact, that the temperature on air-water film interface is assumed same as the temperature of aluminium plate heating up the water film. In reality, the temperature at air-water film interface is slightly lower due to the process of vaporisation. This is illustrated in Figure 24.

Figure 26 compares the outlet temperature dependency on the temperature difference. Outlet temperature is in dimensionless form. For boundary conditions BC1 and BC2, the simulation results and experimental data are within 20% deviation. In the case of boundary condition BC3, the deviation of simulation result from experiment data is higher than 20%.

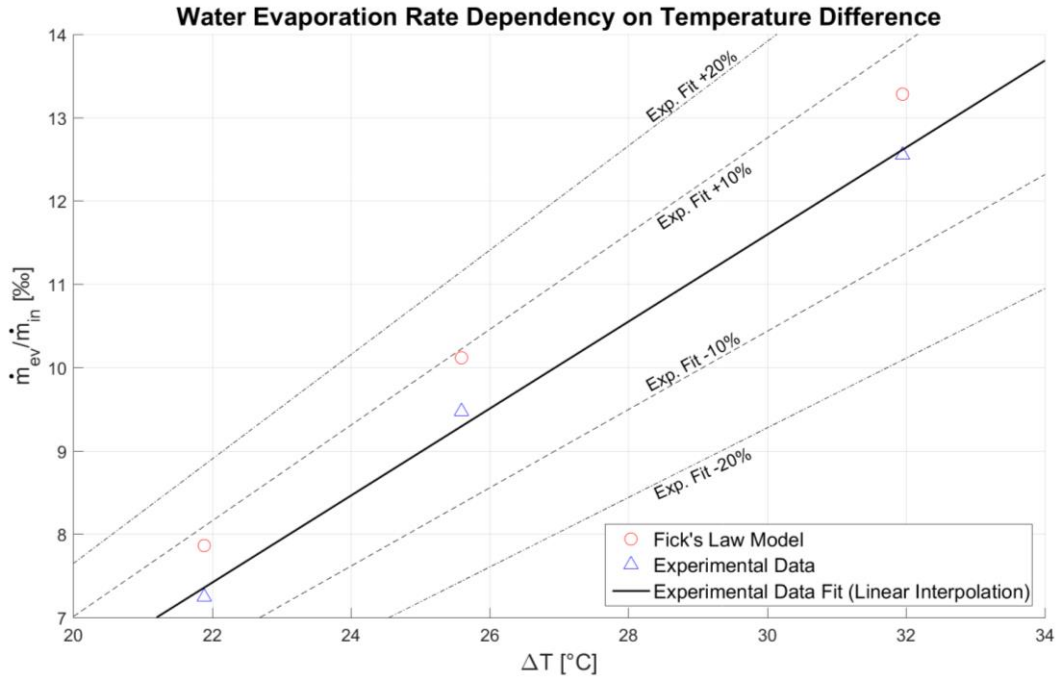

Figure 23 – Water evaporation rate dependency on temperature difference ($T_S - T_{amb}$) (Fick's Law Model).

Figure 29, Figure 32 and Figure 35 show differences of temperature fields experimentally measured and simulated. After comparing experimentally measured and simulated temperature fields for each boundary conditions, it might be concluded that the differences are within an acceptable error and distribution of temperature fields are in good agreement. In top and bottom areas simulation and experiment are slightly different. Simulation is warmer in the top area and colder in bottom area for all three boundary conditions. The warmer area is most likely caused by overestimated value of emissivity and colder area by underestimated value of reflectivity of water film area in simulation settings.

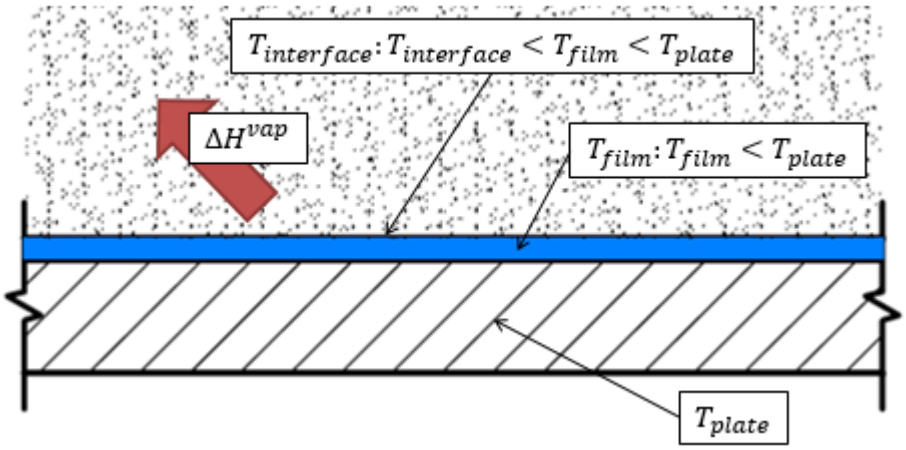

Figure 24 – Scheme of temperature distribution on a plate, water film and air-water film interface.

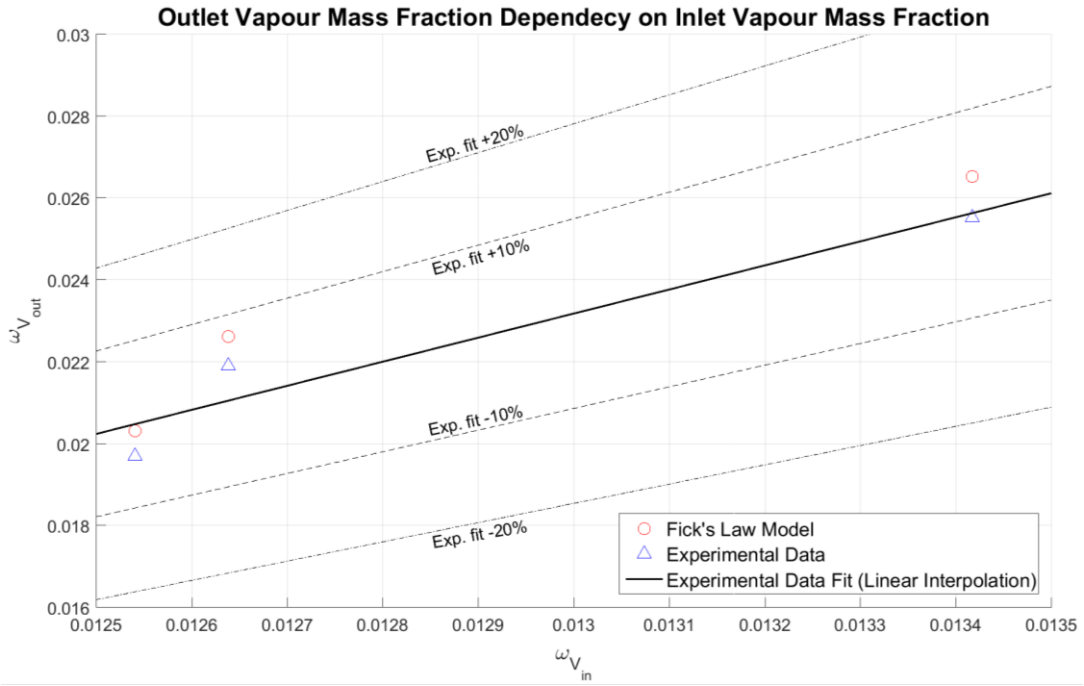

Figure 25 – Outlet vapour mass fraction dependency on an inlet vapour mass fraction (Fick's Law Model).

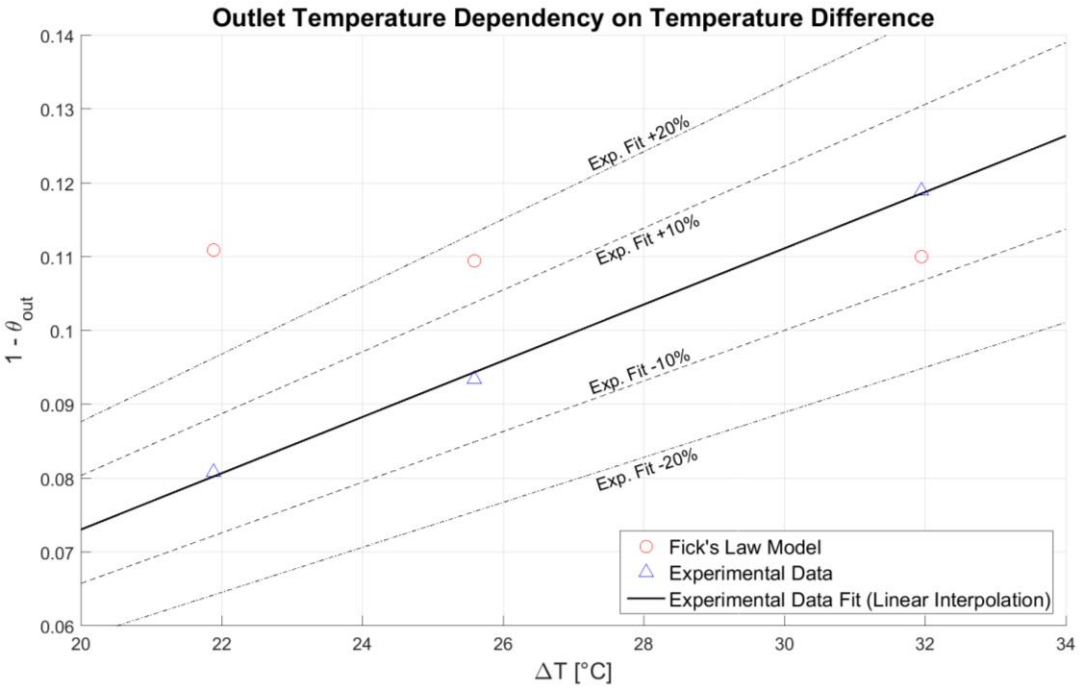

Figure 26 – Outlet temperature dependency on temperature difference ($T_S - T_{amb}$) (Fick's Law Model).

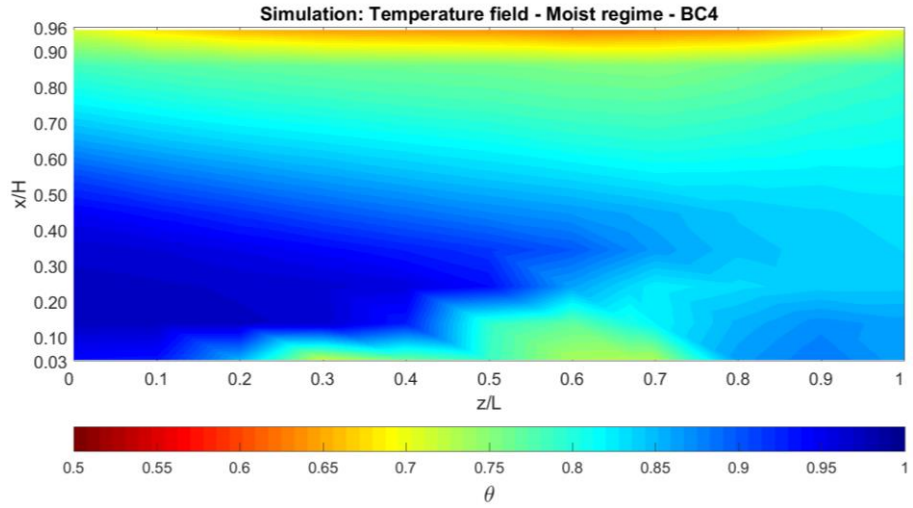

Figure 27 – Simulation temperature field for boundary conditions BC4 (Fick's Law Model).

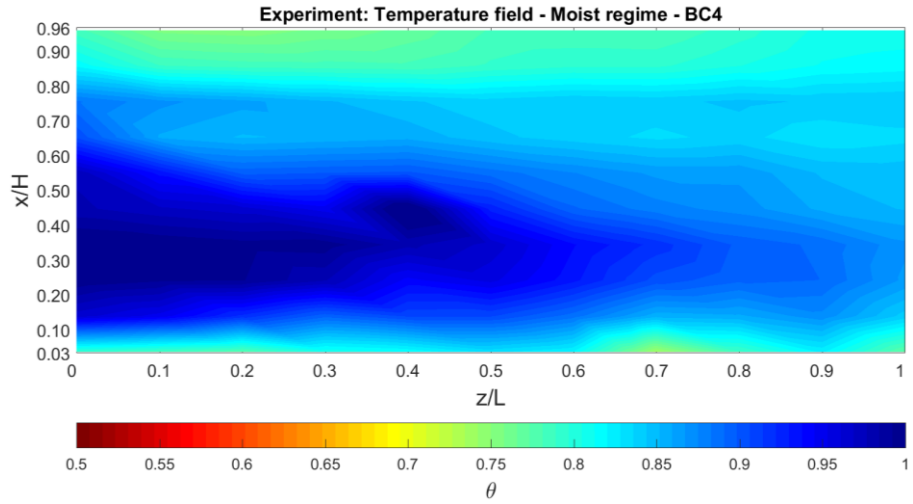

Figure 28 - Experiment temperature field for ambient conditions BC4.

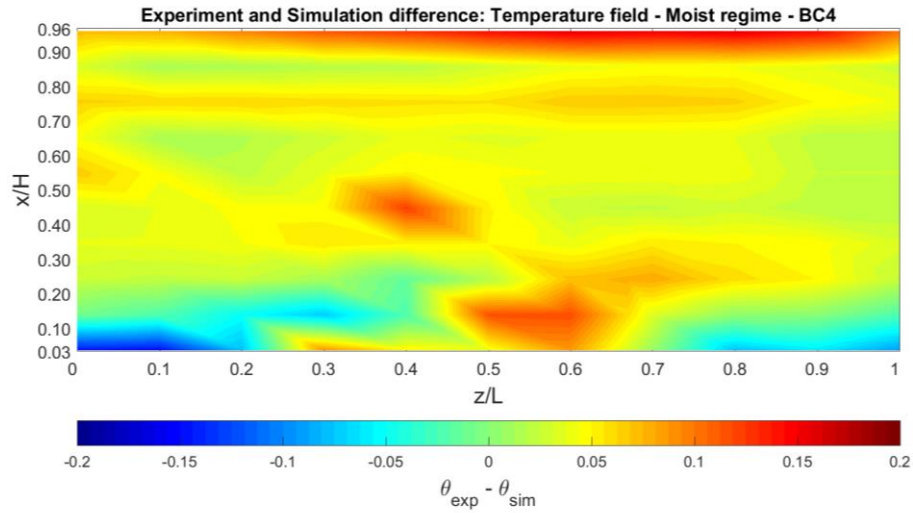

Figure 29 – Simulation (Fick's Law Model) and experiment temperature fields difference for boundary/ambient conditions BC4.

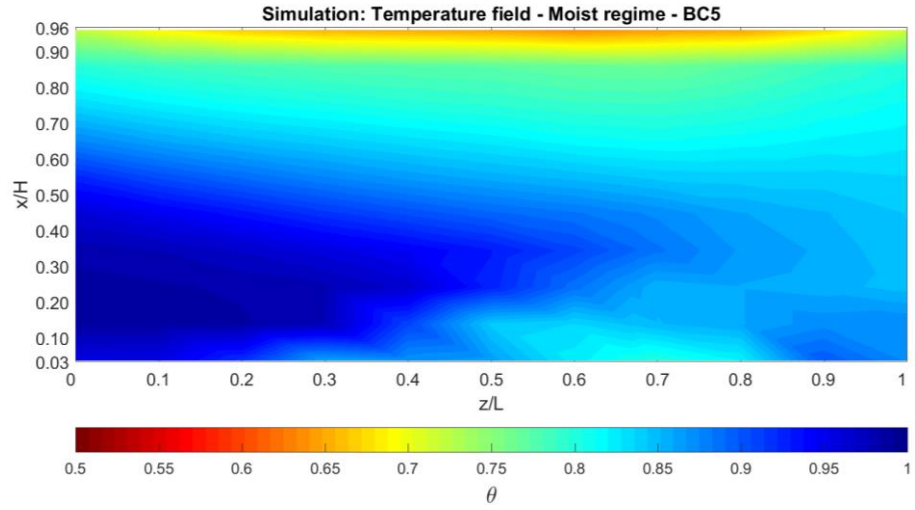

Figure 30 - Simulation temperature field for boundary conditions BC5 (Fick's Law Model).

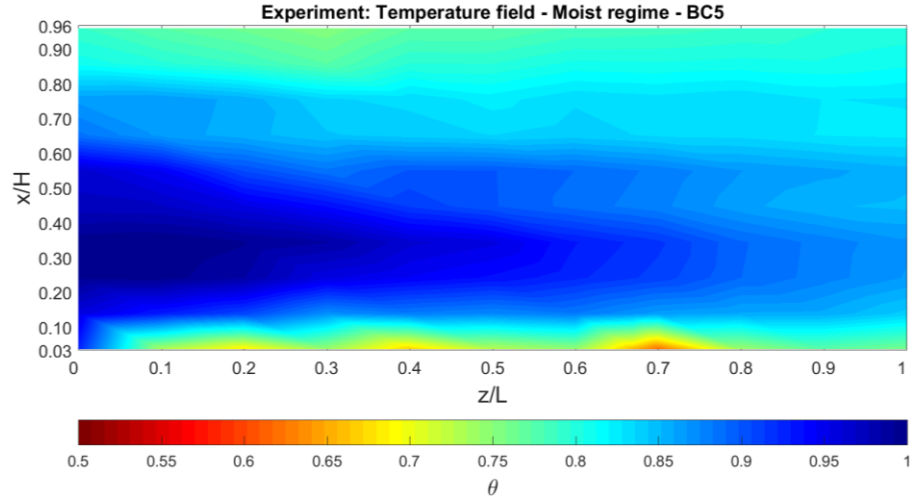

Figure 31 - Experiment temperature field for ambient conditions BC5.

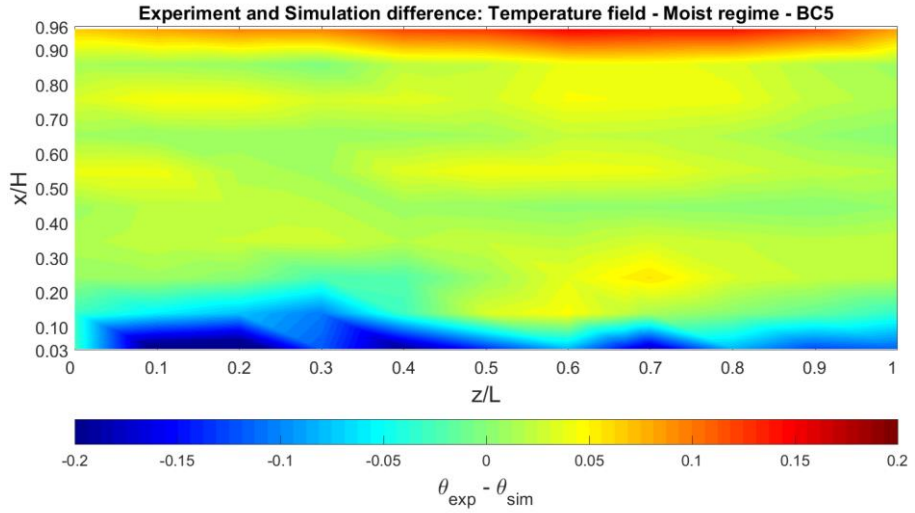

Figure 32 – Simulation (Fick's Law Model) and experiment temperature fields difference for boundary/ambient conditions BC5.

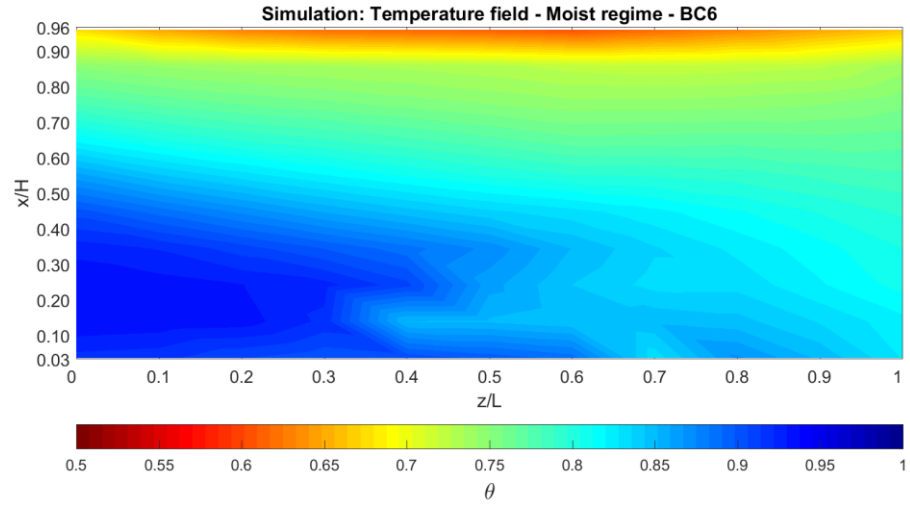

Figure 33 - Simulation temperature field for boundary conditions BC6 (Fick's Law Model).

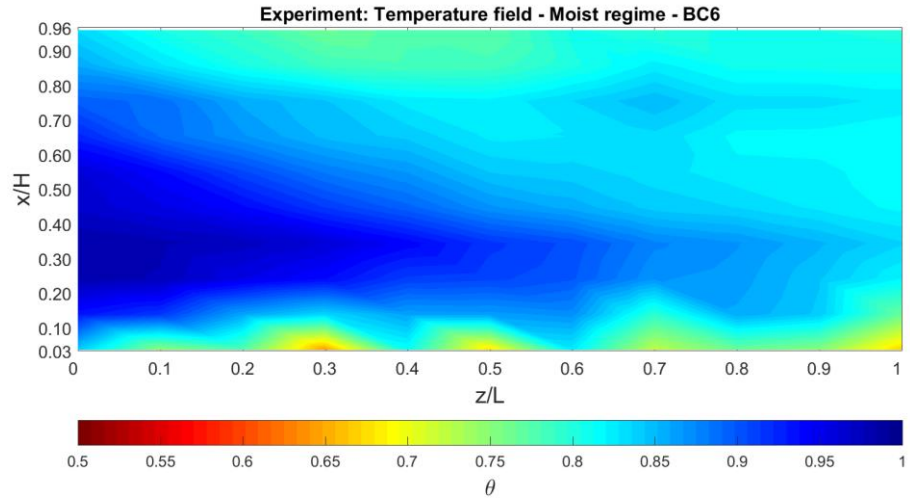

Figure 34 - Experiment temperature field for ambient conditions BC6.

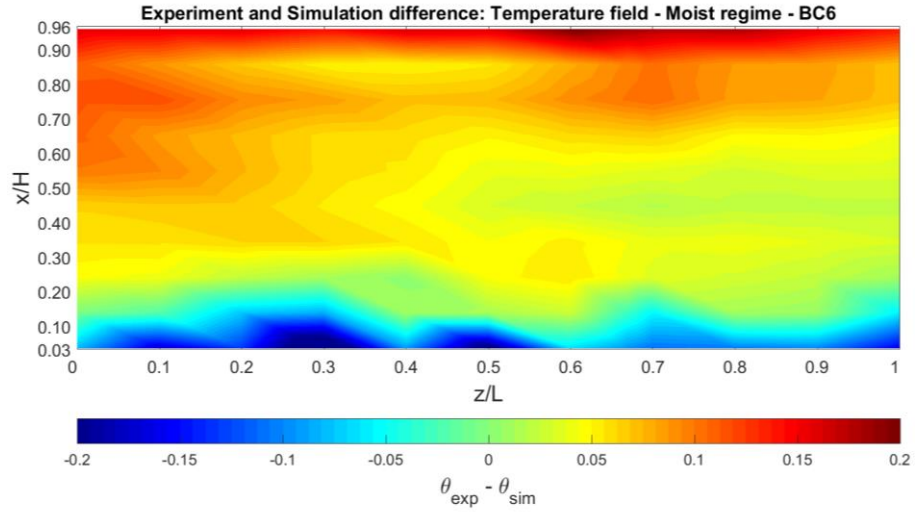

Figure 35 – Simulation (Fick's Law Model) and experiment temperature fields difference for boundary/ambient conditions BC6.

7.3 Post-processing Models

Following part (7.3.1 to 7.3.6) is describing the implementation of the Post-processing Models into STAR-CCM+. It should be remained that Post-processing Models are divided into two sub-approaches: Heat Transfer Analogy Based Model and Lewis Factor Analogy Based Model. In chapter 6.2 were presented the Post-processing Models principles from the theoretical side. Main features of this approach might be recalled as follows:

- The buoyancy caused by natural convection is simulated via defining the user defined equation of state (STAR-CCM+: User Defined EOS). The equation of state employs density variation due to the temperature difference, therefore the advection of the bulk flow is involved. To achieve this, equation (5.1) is adapted.
- Water film is defined as a heat source. Only heat transfer is simulated.
- Water evaporation rate evaluation is based on analogies presented in 6.2.1 and 6.2.2.

7.3.1 Mesh Generation

Table 8 describes parameters of mesh which was generated in STAR-CCM+ and used for final evaluation of Post-processing Models. Values of other parameters which are not mentioned in this table remain set as default.

Table 8 – Setting of used mesh (Post-Processing Models).

Parameters	Values
• **Base Size**	0.011 m
• **Target Surface Size**	80 % of base size
• **Minimum Surface Size**	10 % of base size
• **Surface Growth Rate**	1.2
• **Number of Prism Layers**	13
• **Prism Layer Stretching**	1.1
• **Prism Layer Total Thickness**	0.05175 m
• **Wake Refinement (above fluid film)**	30 % of base size

Since evaluation of the heat transfer coefficient is very important for Post-processing Models, the mesh used is much finer than in the case of the Fick's Law Model. Because of the turbulent modelling involved, there is an additional requirement to size the extrusion layer to achieve $y^+ \approx 1$. The solution dependency on mesh was analysed. Four meshes with different base size were generated. Dependency of water evaporation rate on number of cells can be seen on Figure 36, from which results that mesh with 1 861 742 cells provides convergence.

7.3.2 Boundary Conditions

The water film area is defined as a wall of a given temperature. The temperature is same as the temperature of the plate which is heating up the fluid film. Other boundary conditions are defined in the same way as it is described in 7.1.

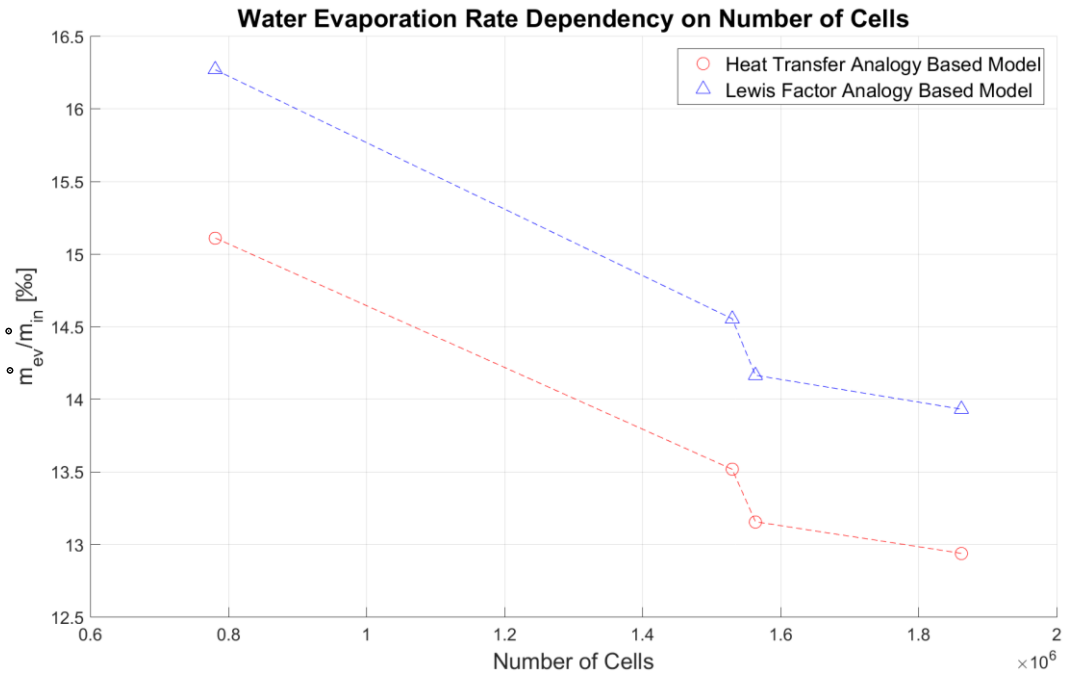

Figure 36 – Water evaporation rate dependency on a number of cells (Post-processing Models).

7.3.3 Simulation Approach

Table 9 lists the simulation setting in the case of Post-processing Models. Instead of Constant Density model *User Defined EOS model* is used. User Defined EOS model allows the user to define arbitrary equation of state of the gas and in the case of Post-processing Models, the equation of state was defined as (5.1). When using the equation (5.1) it is necessary to define the water vapour mass fraction ω_V. The value of water vapour mass fraction ω_V in (5.1) is defined as equivalent to inlet mass fraction of water vapour $\omega_{V_{in}}$ corresponding each boundary condition.

It should be noted that other properties of a single-component gas are defined in the same way as density. In other words, single-component gas properties are defined for a mixture of inlet humidity. This is done since values of density, specific heat capacity and dynamic viscosity influence evaluation of heat transfer coefficient.

The assumption, that the medium in computational domain is incompressible, reduces the overall computational time. This assumption is applicable since differences of absolute pressure are very small.

Evaluation of evaporation rate is employed using two sub-approaches Heat Transfer Analogy Based Model and Lewis Factor Analogy Based Model implemented via User Defined Field Functions. Their principles were presented in chapters 6.2.1 and 6.2.2.

Table 9 – Simulation setting (Post-processing Models).

Models	Parameters
• **Three dimensional**	
• **Steady**	
• **Gas**	Gas Component: Air
• **Non-reacting**	
• **Segregated flow** (Gradients)	Convection: 2nd-order (Gradient Method: Hybrid Gauss-LSQ, Limiter Method: Venkatakrishnan, Custom Accuracy Level Selector: 2.0, Verbose: False; Convection: 2nd-order)
• **User Defined EOS**	Compressible: deactivated
• **Turbulent** (Reynolds-Averaged Navier-Stokes)	
• **k-ε Turbulence** (Realizable k-ε Two-Layer, Exact Wall Distance, Two Layer All y+ Treatment, Exact Wall Treatment)	(Convection: 2nd-order, Curvature Correction Option: Off, Two-Layer Type: Buoyancy Driven(Xu))
• **Gravity**	
• **Segregated Fluid Temperature**	Convection: 2nd-order
• **Radiation**	
• **Surface-to-Surface Radiation** (View Factors Calculator)	
• **Gray Thermal Radiation**	Radiation Temperature: 300.0 K

7.3.4 Continuum Definition

Continuum is assumed as a single-component gas, which properties are defined as it would be a mixture of dry air and water vapour of inlet humidity.

7.3.5 Convergence

Figure 37 presents residual dependency on iteration in the case of Post-processing Models. Residuals decrease satisfies convergence requirement defined in 7.1.2.

Figure 38 shows outlet values and water evaporation rate dependency on iteration, which confirms that simulation reached steady state solution.

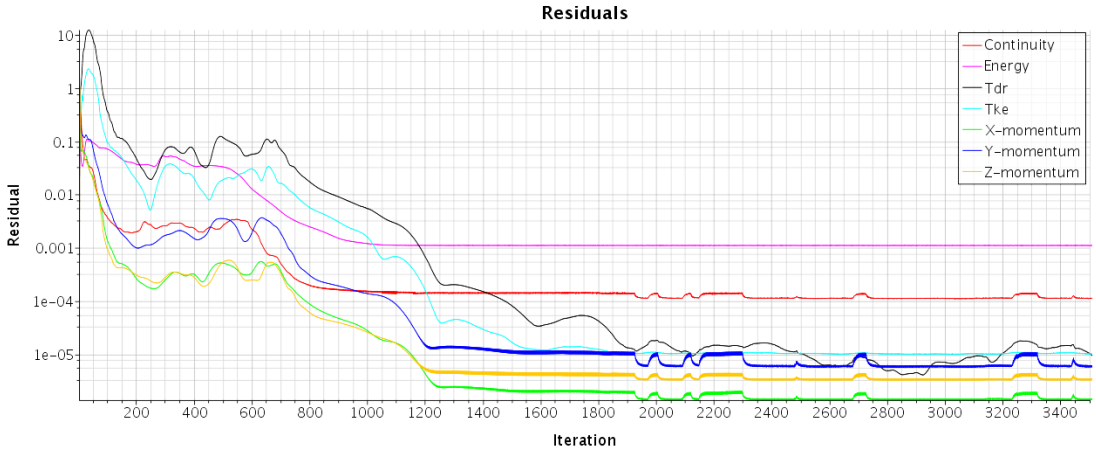

Figure 37 - Residuals dependency on iteration (Post-processing Models).

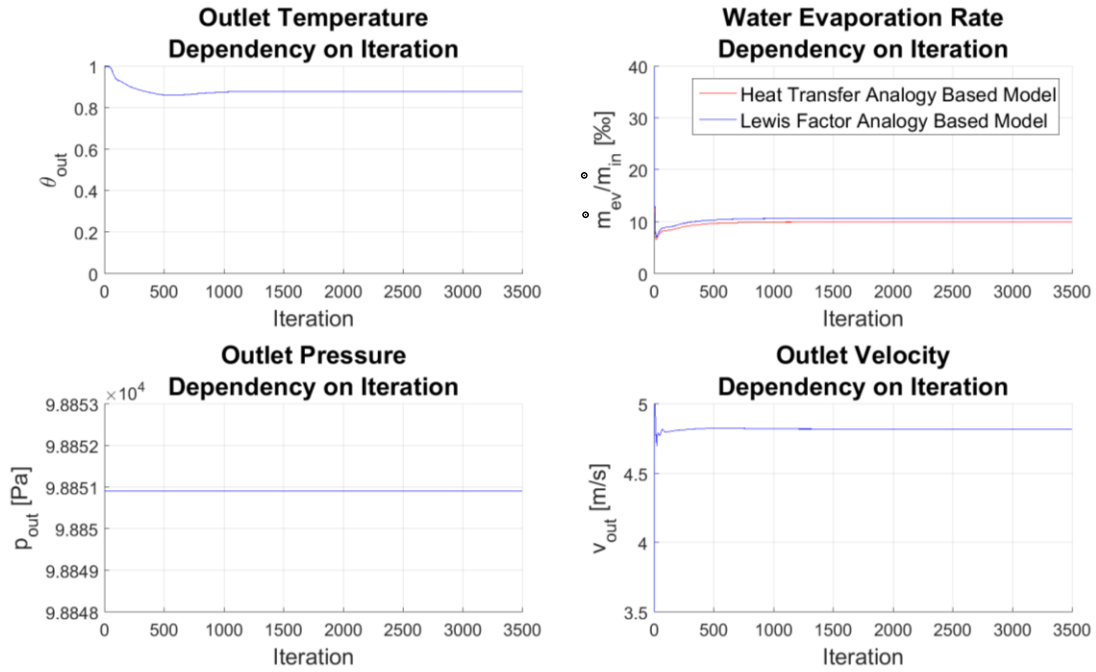

Figure 38 - Monitoring of outlet values and water evaporation rate dependency on iteration (Post-processing Models).

7.3.6 Results

Dependencies presented in figures Figure 39 and Figure 40 are for ranges of $\Delta T \in <20; 34>$ °C, $\dot{m}_{in} \in <0.0104;\ 0.0108>$ and $\omega_{V_{in}} \in <0.0125;\ 0.0134>$ assumed as linearly dependent.

Figure 39 compares results of experimental measurement and results of Post-processing Models (Heat Transfer Analogy Based Model and Lewis Factor Analogy Based Model). It can be seen that results of Post-processing Models are within an acceptable difference from the experiment.

Comparing both sub-approaches, the Lewis Factor Analogy Based Model differs less from the experiment.

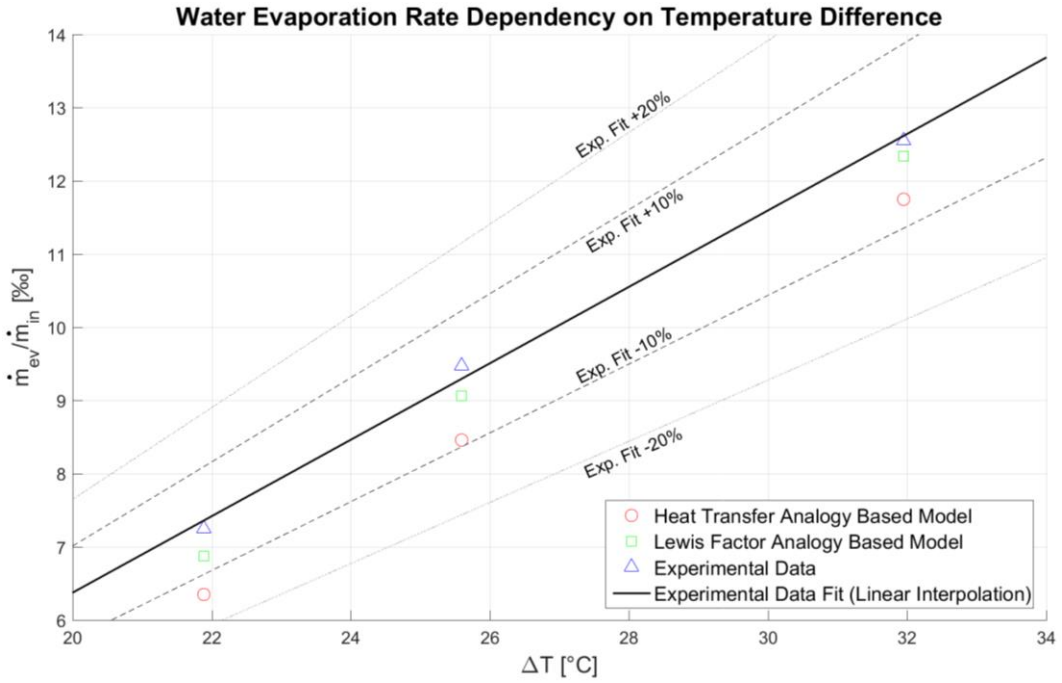

Figure 39 – Water evaporation rate dependency on temperature difference (Post-processing models).

Figure 40 presents the outlet temperature dependency on the temperature difference. Simulation results compared to experimental data are in good agreement. Because of the satisfactory agreement, it might be stated that the evaluation of outlet temperature is not significantly influenced by the assumption of the water film only as a heat source. Assuming the water film area only as a heat source means, that the thermal conductivity of the continuum is constant, which in this case does not influence the evaluation of the outlet temperature.

Figure 41, Figure 44 and Figure 47 show longitudinal temperature fields evaluated by simulation in the case of Post-processing Models. Figure 42, Figure 45 and Figure 48 present longitudinal temperature fields experimentally measured. Simulated and experimentally measured temperature fields are compared in figures Figure 43, Figure 46 and Figure 49. From compared temperature fields might be seen satisfactory agreement in centre areas of the investigated longitudinal plane. In top and bottom part simulation and experiment are a little bit different. Simulation is warmer in the top area and colder in bottom area for all three boundary conditions. The warmer area is most likely caused by overestimated value of emissivity and colder area by underestimated value of reflectivity of water film area in a simulation setting.

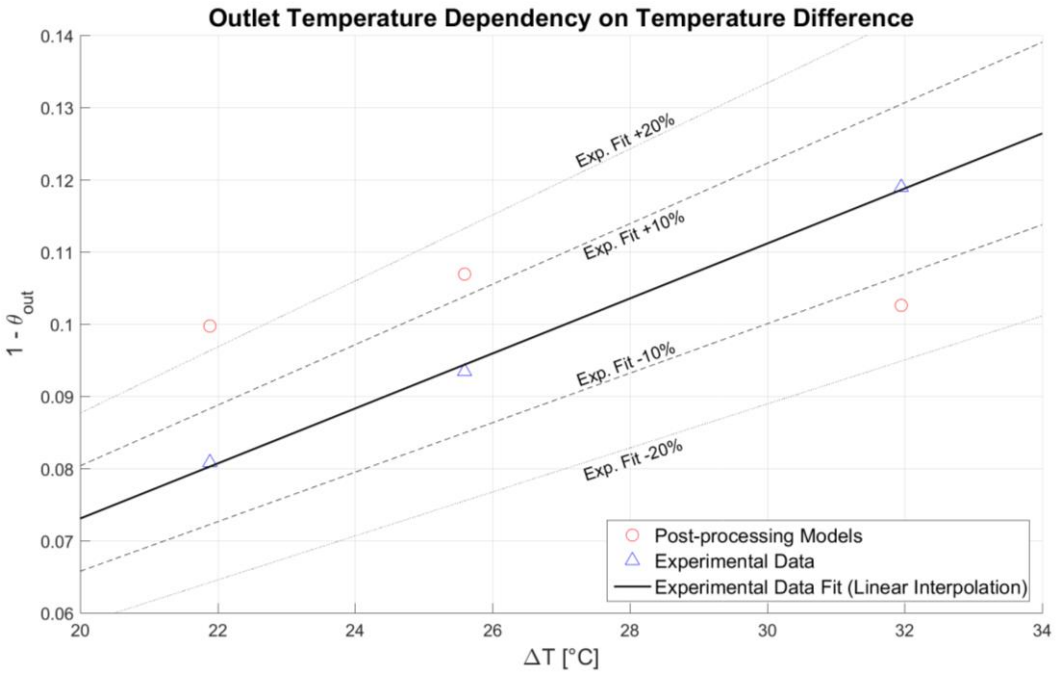

Figure 40 – Outlet temperature dependency on temperature difference (Post-processing Models).

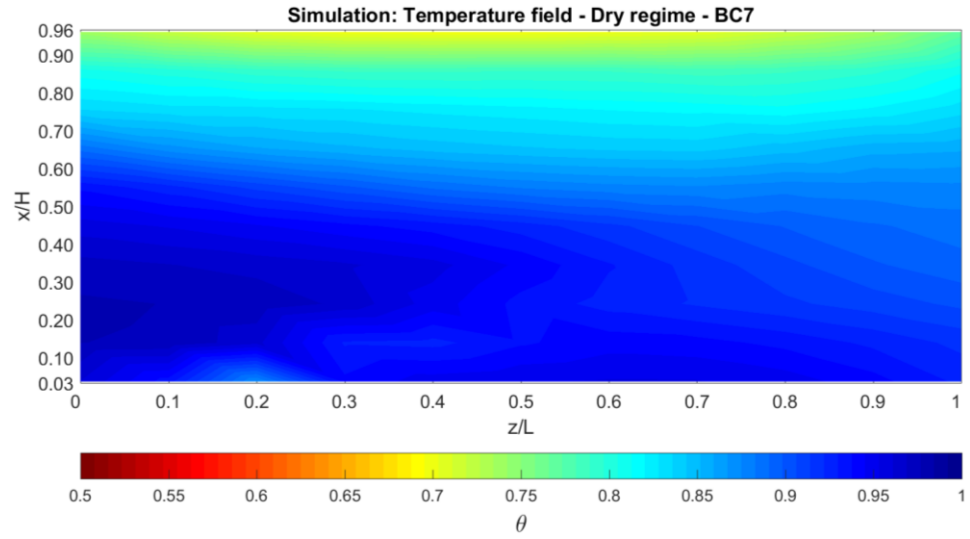

Figure 41 - Simulation temperature field for boundary conditions BC7 (Post-processing Models).

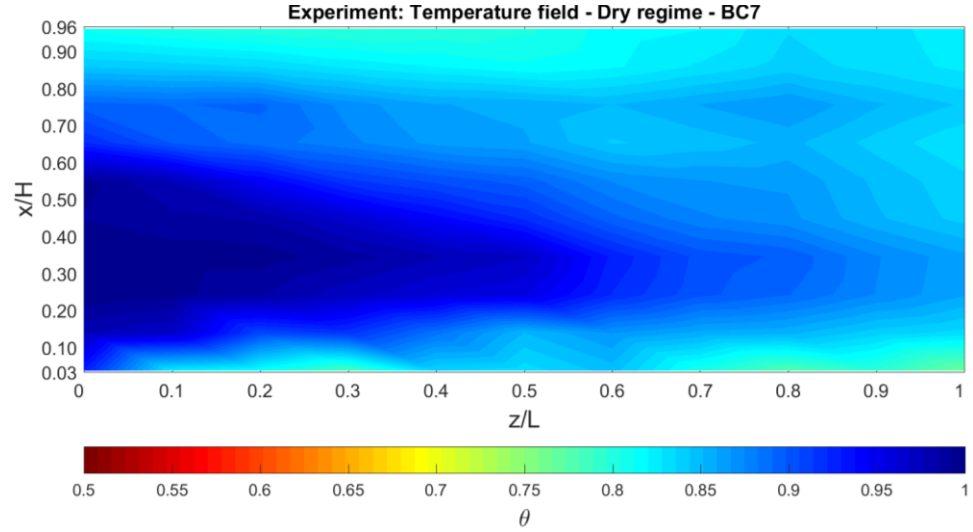

Figure 42 - Experiment temperature field for ambient conditions BC7.

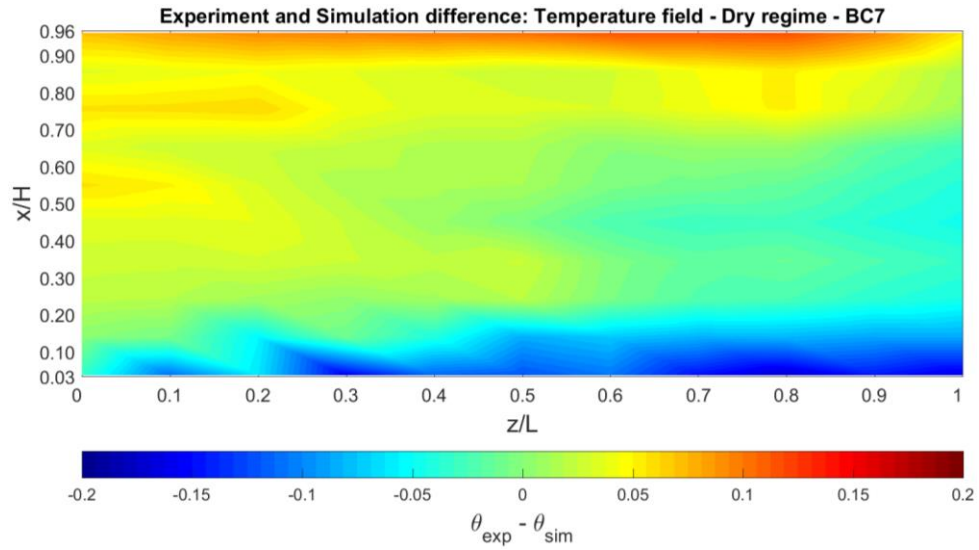

Figure 43 - Simulation (Post-processing Models) and experiment temperature fields difference for boundary/ambient conditions BC7.

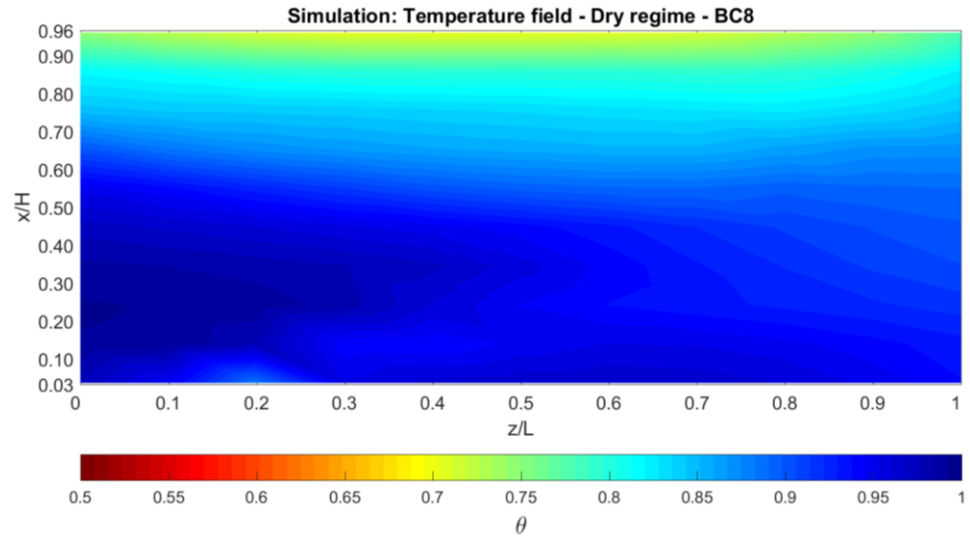

Figure 44 - Simulation temperature field for boundary conditions BC8 (Post-processing Models).

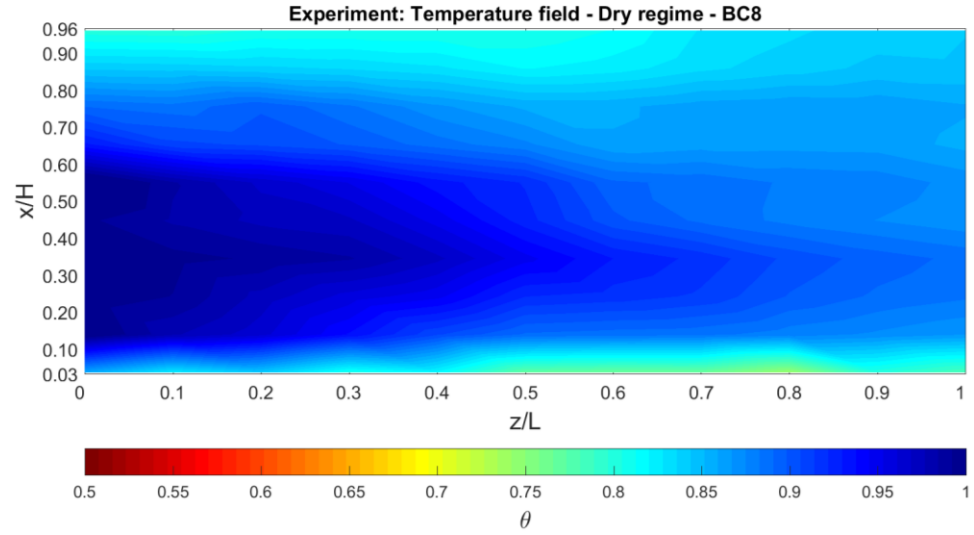

Figure 45 - Experiment temperature field for ambient conditions BC8.

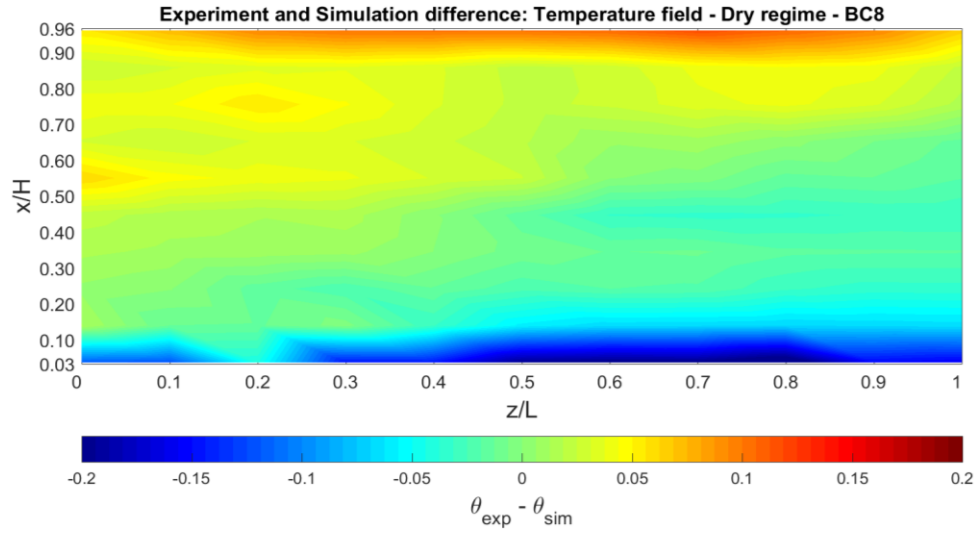

Figure 46 - Simulation (Post-processing Models) and experiment temperature fields difference for boundary/ambient conditions BC8.

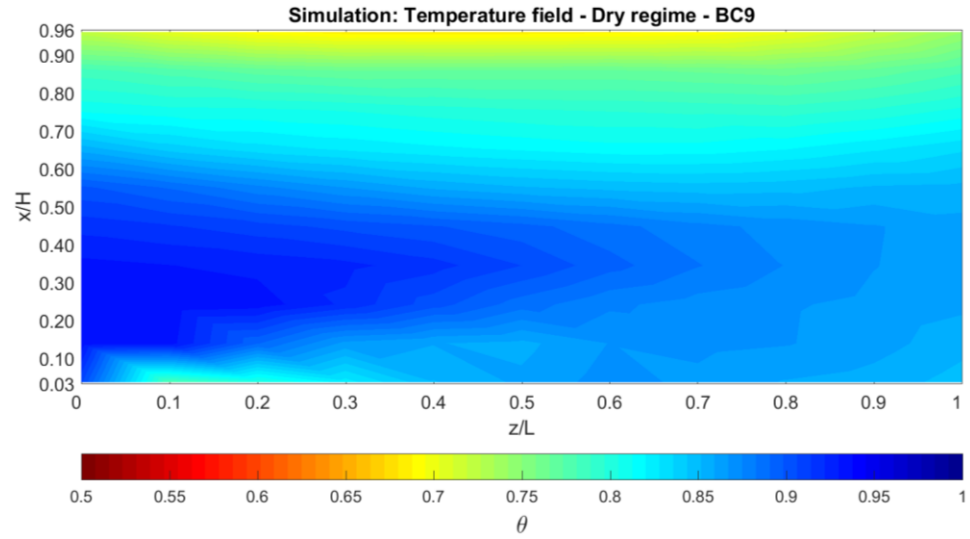

Figure 47 - Simulation temperature field for boundary conditions BC9 (Post-processing Models).

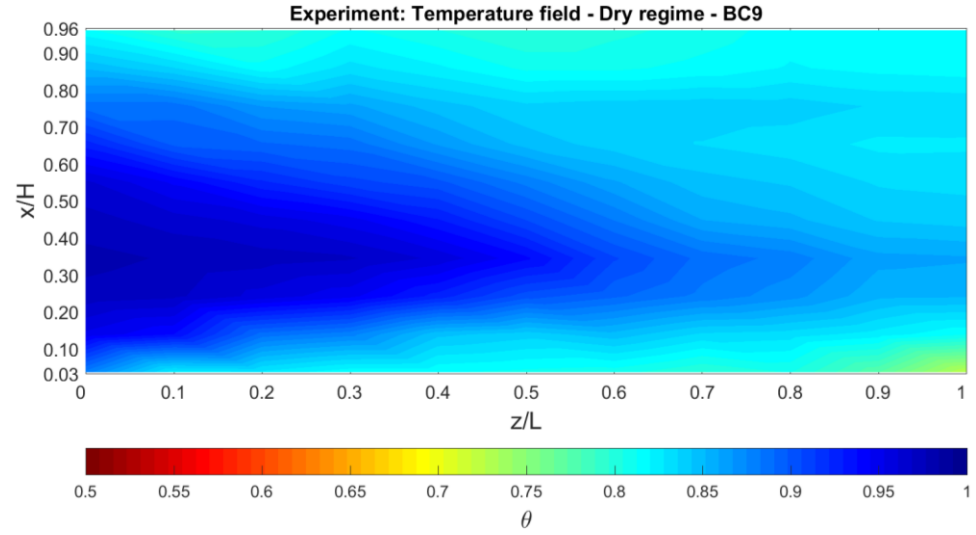

Figure 48 - Experiment temperature field for ambient conditions BC9.

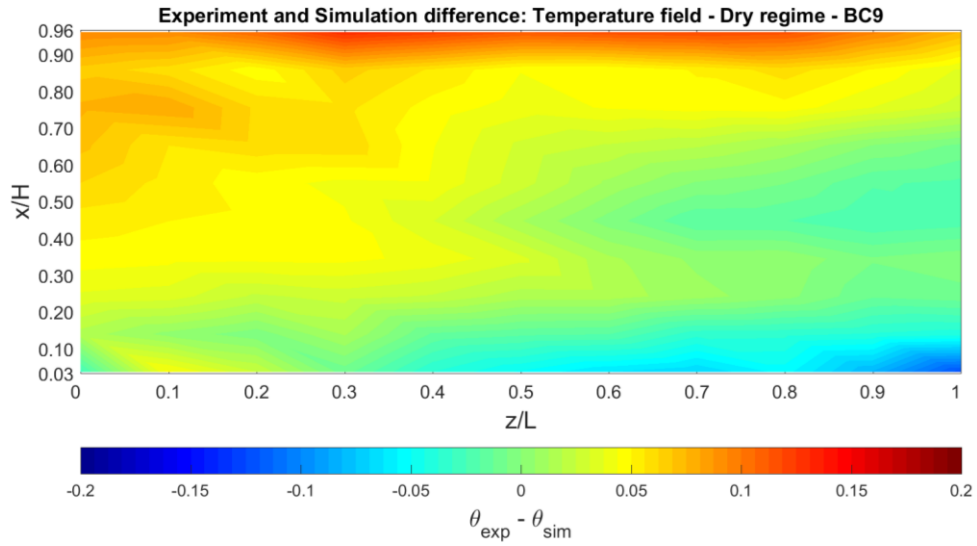

Figure 49 - Simulation (Post-processing Models) and experiment temperature fields difference for boundary/ambient conditions BC9.

8 Developed Models Comparison and Results Discussion

In this chapter are compared models which were investigated in present work, namely Post-Processing Models (Heat Transfer Analogy Based Model, Lewis Factor Analogy Based Model) and Fick's Law Model.

Comparing the models from the point of view of evaluating the water evaporation rate might be seen in Figure 50. From this comparison, can be concluded that the Lewis Factor Analogy Based Model is closest to experimental data. Nevertheless, the overall accuracy of all models is satisfactory.

In the case of Fick's Law Model, the precision could be increased by considering the effect of latent heat of vaporisation. This fact is pointed out and explained in 7.2.6. together with Figure 24.

Recalling 6.2.1 and 6.2.2 it should be noted that the precision of Post-processing models is conditioned to assumptions that $Le = 1$ and $Le_f = 1$, therefore those models should not be applied for problematics in which heat and mass transfer could not be considered equal.

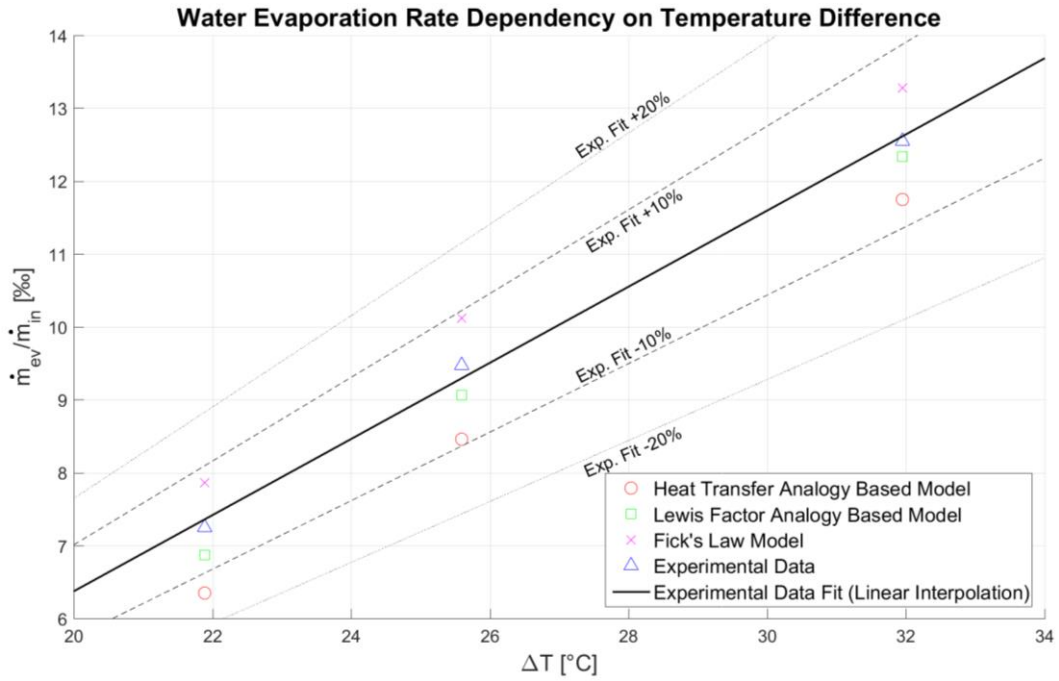

Figure 50 – Water evaporation rate dependency on temperature difference - comparison of Post-Processing Models and Fick's Law Model.

Comparing the models from the point of view of evaluating the outlet temperature might be seen in Figure 51. From this comparison, might be concluded an acceptable agreement of simulation results and experimental data. Outlet temperature evaluated using Post-processing Models is in better agreement with the experimental data than it is in the case of Fick's Law Model. Regarding the precision of simulation results of outlet temperature, should be noted that the quality of mesh was judged only by the dependency of water evaporation rate on a number of cells. To increase the accuracy of simulating the outlet temperature, it would be

necessary to investigate the results dependency on a mesh with respect to the outlet temperature.

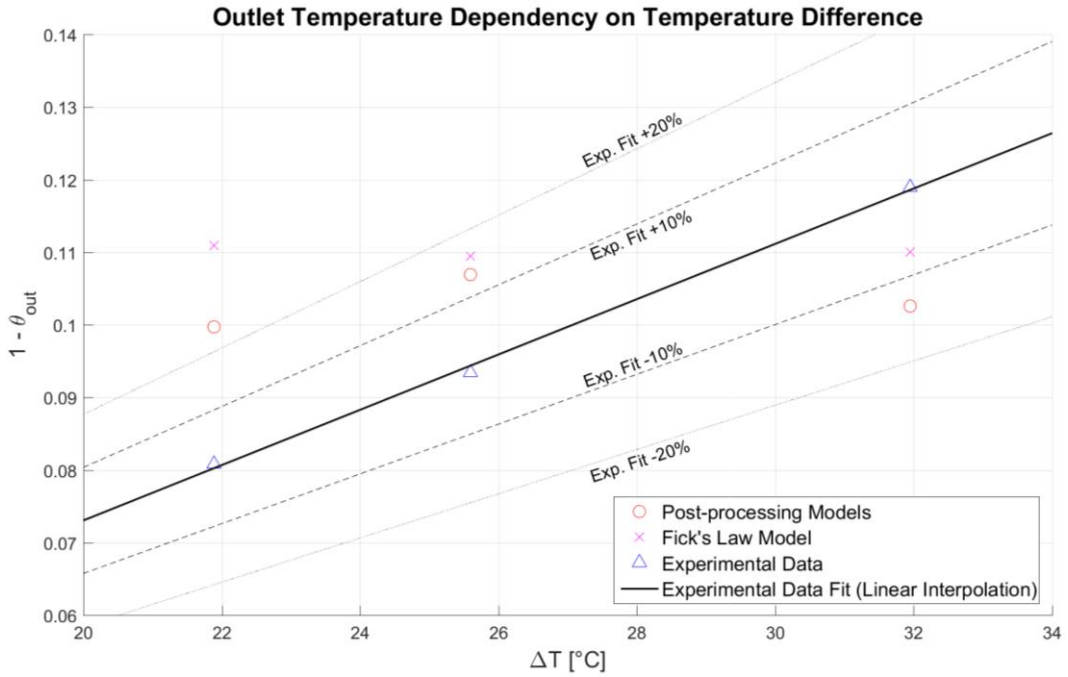

Figure 51 – Outlet temperature dependency on temperature difference – comparison of Post-processing Models and Fick's Law Model.

Recalling the comparison of simulated and experimentally measured temperature fields for both approaches (Post-processing Models and Fick's Law Model), it can be seen that the top and bottom areas of the temperature fields are, respectively, warmer and colder which is caused by overestimating the value of emissivity and underestimating the value of reflectivity, respectively, in the simulations settings.

In the case of the Post-Processing Models, the middle area of the temperature fields is in better agreement with experimental measurement compared with the Fick's Law Model. This fact is a secondary effect of overestimated water evaporation rate by Fick's Law Model. The concentration of the water vapour in the computational domain is higher than it is in the case of the experimental measurement. Because of higher concentration of the water vapour, the thermal diffusivity and thermal conductivity values are lower and that explains, recalling 3.1.1 and 3.1.2, why the simulation is warmer in the middle area.

The fact, that water film area is in the case of Post-processing Models assumed only as a heat source results in limitations. Concentration differences do not contribute to buoyant forces affecting the bulk flow. In other words, in the case of Post-processing Models the buoyant forces are caused only due to the temperature differences, which can lead to underestimated velocity field. This should be kept in mind when evaporation from water film of the large surface area would be simulated.

Regarding the utilisation of both models should be noted that Fick's Law Model is more user-friendly compared with the Post-processing Models. Implementation of momentum source

and defining the fluid film area as a heat and species source is less time-consuming process than the definition of all field functions in case of Post-processing Models.

Coming to mesh requirements of models, the finer mesh is needed in case of Post-Processing Models, which results in increased computational demands. This fact is more obvious from Table 10. Comparison of the total computational time was conducted on a work station (OS: Windows 7; Processor: Intel® Xeon® CPU X5680 @ 3.33GHz (2 processors); Operational memory (RAM): 24 GB) and decomposed into 10 parallel processes for both approaches. Both models were let to compute 3 500 iterations.

Table 10 – Comparison of Fick's Law and Post-processing Models based on a number of cells, total computational time and accuracy. Accuracy is averaged differences of simulation results and experimental data over boundary conditions BC1, BC2 and BC3.

Parameters / Models	Fick's Law Model	Post-processing Models
Number of cells	641 349	1 861 742
Total computational time	2h 37min	6h 46min
Accuracy [%]	+7.08	-3.71 (Lewis Factor Analogy)
		-9.82 (Heat Transfer Analogy)

9 Summary

The thesis deals with the topic of CFD modelling of convective flow over a horizontal water film and its evaporation. Therefore, a related theoretical background such as thermodynamics of moist air and heat and mass transfer theory are presented. Work reviews papers focused on evaporative process (for example: [20], [19], [1] and [2]) and based on those, two independent approaches are investigated and developed – Post-processing Models and Fick's Law Model.

Models of interest (Post-processing Models and Fick's Law Model) are firstly described theoretically, in order to highlight their main principles, and then their implementation into commercial CFD software STAR-CCM+ is shown. The validity of developed models is assessed by comparison with the experimental data and models are compared between each other from the point of view of validity and utilisation.

Development of the Post-processing Models was based on the implementation of heat and mass transfer analogy theory using user field functions in STAR-CCM+. Development of Fick's Law Model was conditioned to the creation of user-coded field function in STAR-CCM+, therefore, it was necessary to manage fundamentals of the C programming language.

The simulation validity was assessed based on a comparison of water evaporation rate, outlet temperature and centre longitudinal temperature field. Additionally, in the case of Fick's Law Model, the outlet humidity was compared. It should be pointed out, that the comparison of simulation results and experimental data of water evaporation rate indicates a very good agreement; the difference of simulation results from the experimental data is on average less than 10% for all presented models. Comparison of simulated and experimentally measured temperature fields are examined. Overall, it is achieved of the acceptable match. Simulation of temperature fields is highly dependent on the definition of radiation properties and how to achieve an even better match is suggested in chapter 8. Simulation results of outlet temperature and outlet humidity are within satisfactory difference from the experiment.

In chapter 8 is pointed out that the Post-processing Models are limited by the assumption that Lewis Number and Lewis Factor equal unity. Regarding the Fick's Law Model, it is mentioned in chapter 8 that the water evaporation rate and outlet humidity are slightly overestimated and possible solution to increase the accuracy is suggested. In other words, in next steps of Fick's Law Model development should be the effect of latent heat of vaporisation added.

Coming to the accomplishment assessment of objectives set for thesis, individual goals are analysed as follows:

- *Discussion of available models applicable in the field of CFD modelling of horizontal water film evaporation.* Available models are discussed in 5.2 and based on their review are described approaches adopted in this work.

- *Description of validation experiment and formulation of the problem for the numerical solution. Description of used mathematical models.* Validation experiment is described in 5.1 and formulation and identification of the problem is presented in 5.1.1. In chapters 6.1 and 6.2 are derived equations related to

investigated phenomena for Fick's Law Model and Post-processing Models, respectively.

- *Development of the post-processing like model and the model based on direct application of Fick's law*. Post-processing like model is in this work denoted as *Post-processing Models* and model based on direct application of Fick's law as *Fick's Law Model.* Both models are developed in this work, firstly, from the theoretical point of view (chapter 6) and later their implementation into STAR-CCM+ is presented (chapter 7).

- *Discussion of an influence of radiation*. The significance of the radiation is mentioned in 3.2, later in 7.1.3 is the radiation influence investigated on the test case, which results in that the radiation cannot be neglected. In chapter 8 is suggested how the radiation properties could be changed in order to achieve of even better temperature field simulation.

- *Testing of an influence of used computational mesh.* For both approaches is tested the mesh influence on the result with the objective to developed mesh-independent solution. Results of this test might be seen in 7.2.1 and 7.3.1 for Fick's Law Model and Post-processing Models, respectively.

- *Discussion of obtained results and comparison of experimental data.* Simulation results are presented in 7.2.6 and 7.3.6 for Fick's Law Model and Post-processing Models, respectively, where results of models are compared with experimental data. Mentioned models are compared between each other and their utilisation is discussed in chapter 8.

Despite the challenging topic, it might be concluded that all thesis goals were successfully accomplished. Developed approaches to modelling horizontal water film evaporation are in the status of possible utilisation for the development of a real product.

References

[1] LAAROUSSI, N., G. LAURIAT a G. DESRAYAUD. Effects of variable density for film evaporation on laminar mixed convection in a vertical channel. *International Journal of Heat and Mass Transfer*. 2009, **52**(1-2), 151-164.

[2] SOSNOWSKI, P., A. PETRONIO a V. ARMENIO. Numerical model for thin film with evaporation and condensation on solid surfaces in systems with conjugated heat transfer. *International Journal of Heat and Mass Transfer*. 2013, **66**, 382-395.

[3] ŠAFAŘÍK, Pavel a Magda VESTFÁLOVÁ. *Termodynamika vlhkého vzduchu*. Praha: Česká technika - nakladatelství ČVUT, 2016. ISBN 978-80-01-06020-9.

[4] JAROSLAV, Chyský. *Vlhký vzduch*. Druhé vydání. Praha: Nakladatelství technické literatury, 1977. ISBN 277386.

[5] CENGEL, Yunus, John CIMBALA a Mehmet KANOGLU. *Fluid Mechanics: Fundamentals and applications*. 2nd ed. New York: McGraw-Hill, 2010. ISBN 9780071284219.

[6] HYHLÍK, Tomáš. *Termodynamické modely proudění vlhkého vzduchu*. Praha, 2016. Habilitační práce. ČVUT v Praze.

[7] CENGEL, Yunus, Robert TURNER a John CIMBALA. *Fundamentals of Thermal-fluid Science*. 3rd ed. New York: McGraw-Hill, 2008. ISBN 0073529257.

[8] *H-x diagram: konstrukce a použití* [online]. Praha, 2000 [cit. 2017-07-10]. Available from: http://homen.vsb.cz/~gal04/Zdenek%20GALDA/VETRANI%20A%20KLIMATIZACE%20I%20(P+K)/CLANKY,%20ODBORNE%20TEXTY/CZ_h-x%20chart%20-%20(by%20SIEMENS).pdf

[9] NOŽIČKA, Jiří. *Základy termomechaniky*. 1. vydání. Praha: Vydavatelství ČVUT, 2001. ISBN 9788001024096.

[10] BERGMAN, T. a Frank INCROPERA. *Fundamentals of Heat and Mass Transfer*. 7th. Hoboken, NJ: Wiley, 2011. ISBN 0470501979.

[11] Thermal Conductivity of Common Materials and Gases. *The Engineering ToolBox* [online]. b.r. [cit. 2017-04-02]. Available from: http://www.engineeringtoolbox.com/thermal-conductivity-d_429.html

[12] KRÖGER, Detlev. *Air-cooled heat exchangers and cooling towers*. Tulsa, Okl.: Penwell Corp., 2004. ISBN 08-781-4896-5.

[13] *The Steve Portal: User Guide* [online]. 2017 [cit. 2017-05-06]. Available from: www.thesteveportal.plm.automation.siemens.com

[14] MORAN, Michael a Howard N. *Fundamentals of Engineering Thermodynamics*. 6th ed. Hoboken: Wiley, 2010. ISBN 9780470540190.

[15] KAYS, W. a M. CRAWFORD. *Convective Heat and Mass Transfer*. 3rd ed. New York: Osborne-McGraw-Hill, 1993. ISBN 0070337217.

[16] SCHLICHTING, H. *Boundary Layer Theory*. 7th edition. New York: McGraw-Hill, 1979. ISBN 978-3540662709.

[17] CLEAR, R. D., L. GARTLAND a F. C. WINKELMANN. *An Empirical Correlation for the Outside Convective Air Film Coefficient for Horizontal Roofs*. Environmental Energy Technologies Division, Lawrence Berkeley National Laboratory, 2001.

[18] BIRD, R., W. STEWART a E. LIGHTFOOT. *Transport Phenomena*. 2nd ed. New York: Wiley, 2007. ISBN 9780470115398.

[19] YAN, W., Y. TSAY a T. LIN. Simultaneous heat and mass transfer in laminar mixed convection flows between vertical parallel plates with asymmetric heating. *Int. J. Heat and Fluid Flow*. 1989, **10**(3), 262-269.

[20] KLOPPERS, Johannes a Detlev KRÖGER. The Lewis factor and its influence on the performance prediction of wet-cooling towers. *International Journal of Thermal Sciences*. 2005, **44**(9), 879-884. DOI: 10.1016/j.ijthermalsci.2005.03.006. ISSN 12900729. Available from: http://linkinghub.elsevier.com/retrieve/pii/S1290072905000943

[21] *Engineering ToolBox* [online]. b.r. [cit. 2017-06-14]. Available from: http://www.engineeringtoolbox.com/emissivity-coefficients-d_447.html

Appendix A

```
#include <math.h>
#include "uclib.h"
#include <time.h>
#include <stdio.h>
#include <stdlib.h>
#include <errno.h>
#include <string.h>

/* Momentum source term involving temperature and solutal differencies */
/* Author: Radomir Kalinay - Created: 14/6/2017                        */

void
MCGB(CoordReal(*result)[3], int size, CoordReal *T, CoordReal *Rho, CoordReal *Ma,
CoordReal *Mh2o, CoordReal *t_ref, CoordReal *MwRef)
{
    int i;

    double gravity[3] = { -9.81, 0.0, 0.0 }; // Defining gravity as vector variable

    double TCoeff = 0.00344; // Defining thermal expansion coefficient
    double TRef = 0.0; // Defining variable
    TRef = t_ref[0]; // Defining reference temperature as scalar value

    double Ma_init = 1-MwRef[0]; // Reference Mass Fraction of Air
    double Mw_init = MwRef[0]; // Reference Mass Fraction of H2O
    double OmRef = (Mw_init / (Ma_init + Mw_init)); // Reference vapour concentration

    double MoA = 28.964; // Molar mass fraction of air
    double MoV = 18.016; // Molar mass fraction of H2O
    double OmCoeff = (MoA/MoV)-1; // Determining vapour expansion coefficient

    /* For loop though all cells */
    for (i = 0; i != size; ++i)
    {
        result[i][0] = (CoordReal)(Rho[i] * gravity[0] * (TCoeff * (TRef - T[i]) +
        OmCoeff * (OmRef - (Mh2o[i] / (Ma[i] + Mh2o[i]))))); // Momentum source in
        x-coordinate
        result[i][1] = (CoordReal)(0); // Momentum source in y-coordinate
        result[i][2] = (CoordReal)(0); // Momentum source in z-coordinate
  }
}

void uclib()
{
  /* Register user functions here */
  ucfunc(MCGB, "VectorFieldFunction", "MCGBoussinesq"); // Parameters of User coded
  field function
  ucarg(MCGB, "Cell", "Temperature", sizeof(CoordReal)); // Calling argument:
  Temperature
  ucarg(MCGB, "Cell", "Density", sizeof(CoordReal)); // Calling argument: Density
  ucarg(MCGB, "Cell", "$MassFractionAir", sizeof(CoordReal)); // Calling argument:
  Mass Fraction of Air
  ucarg(MCGB, "Cell", "$MassFractionH2O", sizeof(CoordReal)); // Calling argument:
  Mass Fraction of H2O
  ucarg(MCGB, "Cell", "$TReff", sizeof(CoordReal)); // Calling argument: Reference
  Temperature = Ambient Temperature
  ucarg(MCGB, "Cell", "$MwReff", sizeof(CoordReal)); // Calling argument: Reference
  Mass Fraction of H2O = Ambient Mass Fraction of H2O
}
```

Figure 52 – C code of momentum source.